Development and Engineering of a cGMP-gated K^+ channel for Optogenetic Silencing

Doctorate thesis

to obtain a doctorate (PhD)

from the Faculty of Medicine

of the University of Bonn

Nidish Ponath Sadanandan

from Mapranam, India

2025

Written with authorization of
the Faculty of Medicine of the University of Bonn

First reviewer: Prof. Dr. Heinz Beck

Second reviewer: Prof. Dr. Günter Mayer

Day of the oral examination: 16/07/2025

From the Max Planck Institute for Neurobiology of Behavior - caesar

Contents

List of Abbreviations

ACR	Anion-conducting Channelrhodopin
AFM	Atomic force microscopy
AP	Action potential
ArchT	Archaerhodopsin
ATP	Adenosine triphosphate
BLINK	Blue-light-induced K^+ channel
BLUF	Sensors of blue-light using flavin-adenine dinucleotide
bPAC	Beggiatoa photoactivated adenylyl cyclase
C1V1	Chimeric Channelrhodopsin from CrChR1 and VcChR1
CA1	Cornu Ammonis Area 1
cAMP	Adenosine 3',5'-cyclic monophosphate
cGMP	Guanosine 3',5'-cyclic monophosphate
ChR	Channelrhodopsin
CNBD	Cyclic nucleotide-binding domain
CNG	Cyclic nucleotide-gated
CNGK	K^+ selective CNG channel
CNs	Cyclic nucleotides
DAPI	4,6 Diaidino-2-phenylindole
eAChR	Engineered anion-selective light-gated ChRs
FA	Formaldehyde
GABA	Gamma-Aminobutyric Acid
GFAP	Glial fibrillary acidic protein
GFP	Green Fluorescent protein
GIRK	G-protein-coupled inwardly rectifying K^+channel
GPCRs	G-protein-coupled receptors

GtACR	Anion-channel Rhodopsins of *Guillardia theta*
h	Hill Coefficient
HcKCR	Kalium Channelrhodopsin of *Hyphochytrium catenoides*
HCN	Hyperpolarization-activated and cyclic nucleotide-modulated
HEK cell	Human embryonic kidney cell
$I_{cGMP/IcAMP}$	Fractional activation by cGMP relative to cAMP
$K_{1/2}$	Half-maximal concentration value
KCRs	Kalium Channelrhodopsin
mV	Millivolt
NaB	Sodium butyrate
NeuN	Neuronal Nuclei Protein
NGS	Normal goat serum
NpHR	Halorhodopsin *Natronomonas pharaonis*
OE-PCR	Overlap extension Polymerase chain reaction
PAC	Photoactivated Adenylyl Cyclase
PBC	Phosphate-binding cassette
PBS	Phosphate Buffered Saline
PDE	Phosphodiesterase
PEI	Polyethylenimine
PLL	Poly-L-Lysine
Po	Open probability
PTLs	Photoswitched tethered ligands
ReaChR	Red-light activatable Channelrhodopsin
RhGC	Rhodopsin Guanylyl Cyclase
ROI	Regions of interest
SD	Standard deviation
SthK	Cyclic nucleotide-gated potassium selective channel of *Spirochaeta thermophila*

TBS-T	Tris-buffered Saline with Triton-X-100
VcChR1	Channelrhodopsin 1 of *Volvox carteri*
VcChR2	Channelrhodopsin 2 of *Volvox carteri*
vRh	Vertebrate Rhodopsins
WiChR	KCR from *Wobblia lunata*
µM	Micromolar
µm	Micrometer
Ω	Ohm

Amino Acids

A / Ala	Alanine
L / Leu	Leucine
R / Arg	Arginine
K / Lys	Lysine
N / Asn	Asparagine
M / Met	Methionine
D / Asp	Aspartic acid
F / Phe	Phenylalanine
C / Cys	Cysteine
P / Pro	Proline
Q / Gln	Glutamine
S / Ser	Serine
E / Glu	Glutamic acid
T / Thr	Threonine
G / Gly	Glycine
W / Tyr	Tryptophan
H / His	Histidine
Y / Tyr	Tyrosine
I / Ile	Isoleucine
V / Val	Valine

1 Introduction

1.1 Optogenetics

To understand the role of specific cell populations in complex biological networks like the brain, highly effective and efficient techniques are needed to manipulate and monitor their behavior. One can for example excite or inhibit a cell type and investigate, how the network reacts to these changes.

Several methods, including genetic, chemical, magnetic, and electrical have been utilized to achieve this goal. While traditional methods like course electrical stimulation can reversibly manipulate neurons, they cannot differentiate between different types of neurons and impact all cells in a given area. On the other hand, pharmacological and genetic manipulations can be customized to cells with specific expression profiles, but they are limited in their temporal and spatial accuracy, often leading to slow kinetics and insufficient reversibility.

Optogenetics has emerged as a popular technique for controlling excitable cells in recent years through the expression of light-sensitive proteins known as Opsins, which can activate or inhibit individual cell types using light. This is a much less invasive approach to activate or inhibit excitable cells like neurons and myocytes with high spatiotemporal resolution. Current optogenetics methodology enables the precise manipulation of individual neurons or populations of neurons in neural circuits. Researchers are using optogenetics to study neural circuits and brain functions. Additionally, optogenetics can be used to study interactions between excitable and non-excitable cells in their natural environment.

The optogenetic toolbox has been vastly expanded since the discovery of light-gated cation

channels called Channelrhodopsins (ChRs) in the green alga *Chlamydomonas reinhardtii* two decades ago (Nagel et al., 2002, 2003). Using ChRs to elicit action potentials (APs) in excitable cells such as the heart and brain is well established (Alfonsa et al., 2015; Berndt et al., 2014; Govorunova et al., 2016; Raimondo et al., 2012). Many different ChR derivatives have been developed or found that activate in response to varying light spectra ranging from blue to red. For example, hybrid ChR1 and ChR2s variants which are redshifted include VChR1, C1v1, ReaChR, Chrimson and bReaChES; (Grosenick et al., 2015; Klapoetke et al., 2014; Lin et al., 2013; Rajasethupathy et al., 2015; Yizhar et al., 2011). These red-shifted variants allow optical stimulation in deeper layers in the brain due to reduced scattering of red-shifted light (Yizhar et al., 2011).

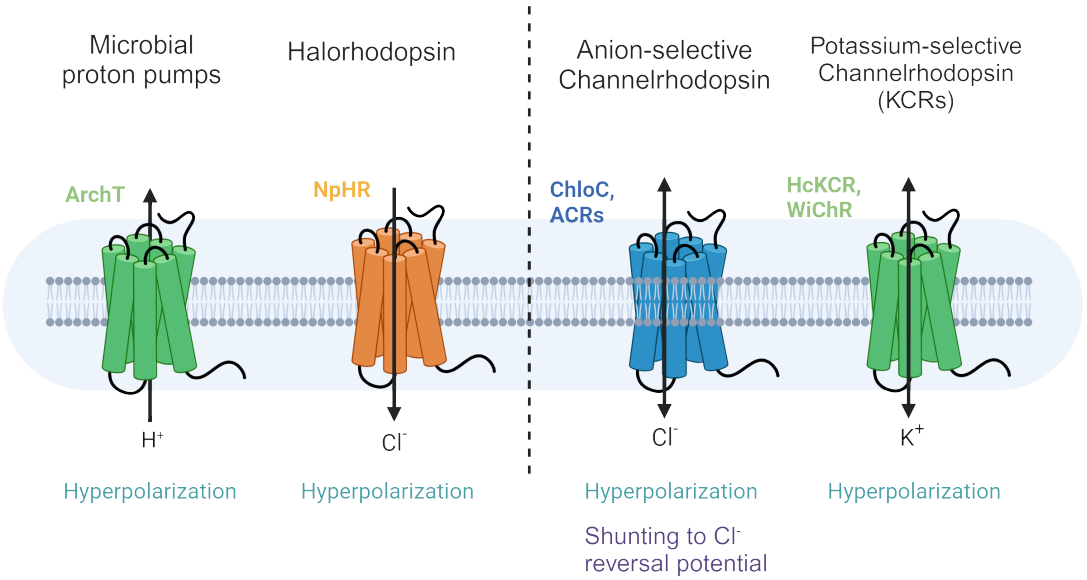

Figure 1.1: Overview of light-gated ion pumps and Channelrhodopsin used in optogenetics for inhibiting action potentials.

While optogenetics offers a plethora of excitatory tools, inhibitory tools remain relatively scarce. Nonetheless, a variety of different optogenetic tools and mechanisms have been reported (Fig 1.1). I will give a broad overview over these techniques with their advantages and disadvantages.

1.1.1 Light-sensitive ion pumps from microbial organisms

In the early days, light-driven ion pumps were used for optogenetic inhibition (Bacteriorhodopsin and Halorhodopsins derivatives). Neural hyperpolarization can be achieved through the transport of anions to the intracellular side or by the extrusion of cations or protons from the intracellular to the extracellular space. In 2007, the light-driven, inward-directed chloride (Cl^-) pump, Halorhodopsin (NpHR) from *Natronomonas pharaonis* was employed to inhibit action potential (AP) firing in neurons. (Gradinaru et al., 2008; Han & Boyden, 2007; Zhang et al., 2007). Also the light-driven outward-directed proton pump Archaerhodopsin (ArchT) from *Halorubrum sodomense* (Chow et al., 2010) and the sodium pump KR2 (Inoue et al., 2013) entered the pool of inhibitory tools. KR2 inhibits AP generation without significantly altering ion gradients *in vitro*, but their efficiency in situ is insufficient due to small photocurrents (Grimm et al., 2018; Tsunoda et al., 2017). Modified versions of microbial ion-pumping Rhodopsin variants, such as eNpHR3.0 and eArch3.0, are widely used to hyperpolarize neurons. However, their utility is limited to silencing for over only a few seconds.

1.1.2 Light-Gated Ion Channels

Other inhibitory tools utilize ion channels, which rely on the electrochemical gradient for ion exchange. In order to silence neurons, light-gated ion channels that are selective for potassium (K^+) or chloride (Cl^-) would be ideal. In mature neurons, the Cl^- and K^+ reversal potentials are typically close to or more negative than the resting membrane potential, which usually ranges between -65 mV and -75 mV. When light-gated Cl^- or K^+ channels open, they effectively ’shunt’ membrane depolarization, thereby preventing the generation of new AP. Additionally, ion channels are advantageous because they conduct many ions per absorbed photon through the gradient across the membrane.

1.1.2.1 eACRs - Engineered Anion-Conducting Channelrhodopsins

Structural details from the high-resolution crystal structure of C1C2, a chimera between ChR1 and ChR2 from *Chlamydomonas reinhardtii* (Kato et al., 2012), provided crucial structural details that enabled scientists to transform naturally occurring light-gated cation-selective ChR variants into engineered anion-selective light-gated ChRs (eAChR). This breakthrough has led to the development of a new category of optogenetic silencing tools. Various mutational strategies were deployed to develop ChR variants with enhanced anion selectivity (Berndt et al., 2014; Wietek et al., 2014). However, a residual H^+conductance rendered these early engineered anion-conducting ChRs (eACRs) of limited use as silencing tools. In the later stage of optimization, it was realized that it was necessary to reduce the residual proton conductance; these efforts yielded iC++ and iChloC, two highly anion-selective eACRs with slow closing kinetics and reduced photon budget (Berndt et al., 2014; Wietek et al., 2015), and ZipACR, which allows for optical inhibition of individual neuronal spikes at high frequencies (Govorunova et al., 2017). ZipACR is a spectrally shifted version of eACRs.

1.1.2.2 nACRs – Natural Anion-Conducting Channelrhodopsins

In recent years, new screening efforts have resulted in the discovery of a new category of natural ACRs (nACRs) with its founding member identified in the cryptophyte alga *Guillardia theta*. By now, the cryptophyte ACR family has expanded to 20 members (Govorunova et al., 2017), including the Rhodopsin channels GtACR1 and GtACR2. These channels are derived from *Guillardia theta* and exhibit almost perfect anion selectivity. Moreover, they produce several-fold larger photocurrents in mammalian cells than any of the eACRs (Govorunova et al., 2016), with a larger single-channel conductance (Sineshchekov et al., 2015).

The advantage of ACRs is their mode of inhibition that results in shunting of the membrane potential, similar to $GABA_A$ receptors. ACRs with slow off-kinetics are of particular interest

when prolonged silencing is required. Nevertheless, long-lasting activation of ACRs can shift Cl^- gradients and the reversal potential accordingly. Any such ACR-mediated Cl^- accumulation reduces the AP threshold and changes cell excitability (Alfonsa et al., 2015; Sørensen et al., 2018; Staley et al., 1995). Also, when the intracellular Cl^- concentration of a cell is high, activation of ACR produces excitation instead of inhibition, as is the case for immature neurons; also some neuronal compartments such as axons and presynaptic terminals have been suggested to contain elevated chloride levels (Szabadics et al., 2006; Turecek & Trussell, 2001). Thus, ACRs are promising optogenetic tools for inhibition only for adult neurons and when targeted to neuronal soma (Mahn et al., 2018).

1.1.2.3 KCRs – Kalium Channelrhodopsins

Kalium Channelrhodopsin (KCRs) form a new group of light-gated K^+ channels that have the potential of overcoming many of the limitations of previously mentioned optogenetic inhibitors, as K^+ currents underlie the resting state of almost all excitable cells. Recently, two Channelrhodopsins that naturally conduct potassium have been identified in the stramenopile *Hyphochytrium catenoides* (HcKCR1 and HcKCR2) and were used for inhibitory purposes (Govorunova et al., 2021). WiChR from *Wobblia lunata* is a KCR with improved K^+ selectivity, and higher light sensitivity compared with other KCRs. WiChR allows single- and two-photon inhibition at low irradiance, making it an efficient inhibitor (Vierock et al., 2022).

1.1.3 Light-activated G-protein-coupled receptors

Light-activated G-protein-coupled receptors (GPCRs) possess inhibitory properties similar to Rhodopsin pumps and ACRs. GPCRs are proteins that have seven transmembrane domains and interact with heterotrimeric G proteins or β-arrestin. The α subunits of G proteins fall into four categories: Gi/o, Gs, Gq/11, and G12/13 (Wettschureck & Offermanns, 2005). In the perspective of neuronal silencing, Gi/o works by reducing Adenylyl Cyclase activity, blocking P/Q- and N-type calcium channels, and activating endogenous mammalian

G-protein-coupled inwardly rectifying K^+ (GIRK) channels (Dutar et al., 2000). This results in the inhibitory modulation of synaptic transmission (Wettschureck & Offermanns, 2005).

Type-II Rhodopsins, which mediate vision in vertebrates, are G-protein-coupled receptors activated by light. Vertebrate Rhodopsins (vRh) from rod cells, which interact with Gi/o proteins, are responsible for this process. In fact, vRh-4 (RO4) was the first light-sensitive protein ever employed to reduce neuronal excitability in mammalian neurons *in vivo*, as reported (Li et al., 2005). One potential issue with RO4 is that it requires a continuous supply of 11-cis-retinal, which is not always available. However, this is not a problem in the mammalian brain because cis-retinal is abundant there.

Recent advancements have led to develpoment of two novel photo-switchable G protein-coupled receptor (GPCR)-based opsins designed for the rapid and reversible optical control of the inhibitory Gi/o protein signaling pathway. The first, termed eOPN3, is derived from a mosquito homolog of mammalian Encephalopsin (Mahn et al., 2021). The second, known as lamprey Parapinopsin (PPO), was identified by Copits et al., 2021. Both eOPN3 and PPO have demonstrated efficacy in inhibiting neurotransmitter release at the presynaptic level by decreasing the probability of neurotransmitter vesicle release. These light-activated GPCR tools provide innovative opportunities for silencing axonal projections and modulating synaptic transmission with high spatiotemporal precision. However, compared with other optogentic tools, eOPN3 and PPO exhibit reduced effectiveness in somatic inhibition. The manipulation of neuronal activity through Gi/o-mediated inhibition is contingent upon the intracellular content of G-proteins and other effector proteins, which can differ across various cell types and subcellular compartments.

1.1.4 Other Combined Inhibitory Tools

Another approach to silencing neuronal activity is by covalently attaching synthetic photoswitched tethered ligands (PTLs) to either natural or chimeric K^+ channels, which yielded the tools SPARK (Banghart et al., 2004) and HyLighter (Janovjak et al., 2010), respec-

tively. PTL-gated K^+ channels allow reversible activation and inactivation of a K^+ current upon illumination, however, the requirement to deliver an additional cofactor has impacted their widespread application. With a similar concept, but with a natural cofactor, the blue-light-activated K^+ channel BLINK (Cosentino et al., 2015), consisting of the photosensory domain LOV2 fused to the small viral K^+ channel Kcv was engineered. BLINK channels initially faced issues with expression, but the second version BLINK 2 improved on this respect. The major drawback of the BLINK1/2 system was a very slow time course of activation and deactivation, which is in the minute range (Alberio et al., 2018).

1.2 K^+ Channel based Two-Component System PACK and SthK/bP

Another system that was recently presented was a K^+ channel based two-component hyperpolarizing tool SthK-bP and PACK which is based on a combination of a Photoactivated Adenylyl Cyclase (PAC) from soil bacterium *Beggiatoa* (bPAC) with a small cAMP-gated K^+ channel (SthK) from *Spirochaeta thermophila* (Beck et al., 2018; Bernal Sierra et al., 2018). Blue light activates either a soluble or channel-linked variant of bPAC, which converts adenosine triphosphate (ATP) to cyclic adenosine monophosphate (cAMP). The cAMP then binds to the SthK channel, resulting in K^+ efflux and subsequent hyperpolarization (Fig 1.2). The silencing efficacy of both tools has been shown in various in- vivo models. The PACK system was used to suppress hippocampal CA1 unit activity in anaesthetized mice (Bernal Sierra et al., 2018) and *Drosophila* larvae (Beck et al., 2018) and it inhibited spontaneous coiling of zebrafish larvae when expressed in motoneurons. In addition, the PACK system inhibited spiking in cultured cardiomyocytes from rabbit (Bernal Sierra et al., 2018).

PACK can transport considerably more charges per absorbed photon than ArchT and *Gt*ACR1 (up to a factor of 3×10^4 and 6.8×10^2, respectively) (Bernal Sierra et al., 2018). Despite the high efficiency in silencing excitable cells, the PACK system is limited by slow on- and off-kinetics of light-induced currents caused by intrinsically slow photocycle kinetics

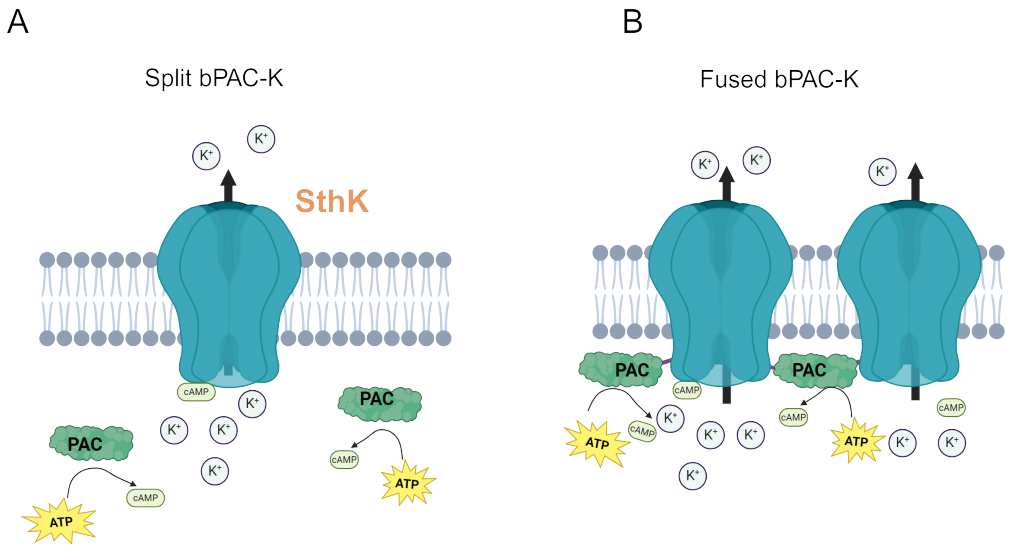

Figure 1.2: K^+-Channel based two-component hyperpolarizing tool systems. A. Schematic of the split-PACK and fused-PACK B. construct design for SthK coexpression with PACs.

of PAC and cAMP turnover in the target cells. In addition, the system may evoke undesired cAMP-induced side-effects on intracellular signaling cascades, metabolism and gene expression; a recent study showed that in long-term use of PACK in the mouse hippocampus, cellular dispersion and astrogliosis occurs (Kleis et al., 2022).

In order to overcome the limitations of cAMP as the second messenger for the two-component inhibitory tool, we reasoned that a combination of a light-activated Guanylate Cyclase (Rhodopsin GC) (Fischer et al., 2021; Scheib et al., 2018) with a cGMP-activated K^+ channel might be advantageous, as cGMP is used in much fewer cells. My task was to engineer a cGMP-gated K^+ channel that is capable of inhibiting excitable cells when activated indirectly via Rhodopsin GC.

As a candidate, I chose the SthK channel, the cyclic nucleotide-gated channel from the thermophilic bacteria *Spirochaeta thermophila*, because it is relatively small and expresses well in heterologous systems (Brams et al., 2014; Henß et al., 2022). Its disadvantage for the current project is the utterly bad performance during activation with cGMP. In fact, in

the original characterization of the SthK channel, cGMP was considered a competitive antagonist. Only later it was demonstrated, that cGMP does activate the channel, albeit with very low efficacy. I will give an overview over the latest research on the SthK channel with a focus on structural studies that try to explain its binding and activation properties.

1.3 SthK from *Spirochaeta thermophila*

The SthK channel has served as a model system for deciphering the intricate channel-gating mechanisms of the homologous cyclic nucleotide-gated (CNG) and hyperpolarization-activated and cyclic nucleotide-modulated (HCN) channels in molecular detail (Andersson et al., 2023; Brams et al., 2014; Evans et al., 2020; Kaupp & Seifert, 2002; Kesters et al., 2015; Marchesi et al., 2018; Morgan et al., 2019; Rheinberger et al., 2018; Schmidpeter & Nimigean, 2021; Schmidpeter et al., 2018, 2020). In *Spirochaete thermophila* bacteria, these channels facilitate ion flow across the cell membrane and regulate homeostasis.

Structural studies on the SthK channel have provided significant insight into its function and mechanism. Key studies have utilized techniques like cryo-electron microscopy and x-ray crystallography to determine a high-resolution structure of the channel in the apo, cAMP bound, and cGMP bound states. These studies revealed how the ligand binding induces the changes that open the channel (Kesters et al., 2015; Marchesi et al., 2018; Schmidpeter et al., 2018).

1.3.1 Structure of the SthK channel

The SthK channel is made up of four identical subunits, which form a symmetric tetramer (Fig 1.3). The channel has an ion-conducting pore along the four-fold axis. Each subunit is composed of six transmembrane helices followed by a large cytoplasmic region. Within the transmembrane region, the voltage-sensing domain is made up of S1-S4, while the pore domain is made up of S5 and S6, with the selectivity filter located between these two helices. After the transmembrane region, there is a C-linker domain composed of six he-

lices, followed by a cyclic nucleotide-binding domain (CNBD), which contains four helices (A-C and P) and a β-roll. The C-linker domain makes extensive inter-subunit contacts, with the A' and B' helices of one subunit resting on the C' and D' helices of the adjacent subunit (clockwise if viewed from the extracellular side) in an "elbow on the shoulder" configuration (Li et al., 2017; Morgan et al., 2019; Rheinberger et al., 2018; Zagotta et al., 2003).

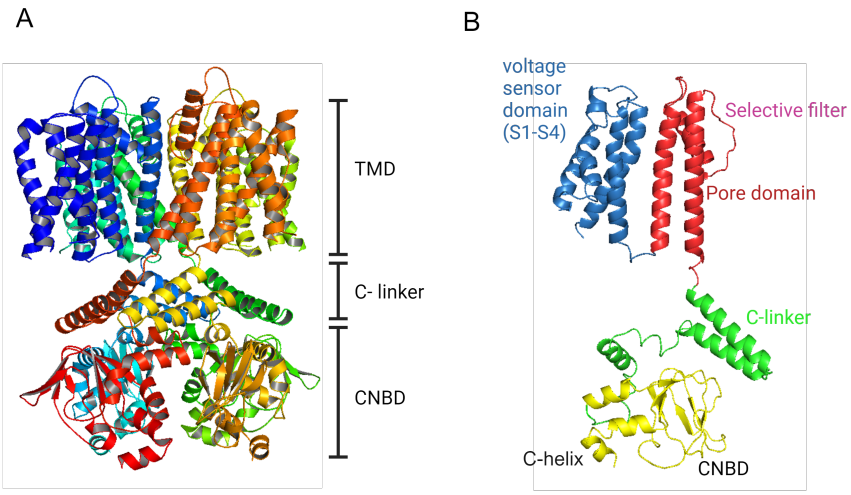

Figure 1.3: A. Cartoon representation of the SthK channel tetramer. B. Cartoon representation of single subunit with transmembrane domain S1-S4 (blue), S5-S6 (red), C-linker (green) and CNBD domain (yellow).

Structural studies provided deep insight into the conformational changes of the SthK channel upon binding cyclic nucleotide. This mechanism involves a series of conformational changes initiated by cyclic nucleotide binding. First, the ligand binds to the phosphate-binding cassette (PBC). PBC is a region within the β-roll of the CNBD that binds to the phosphate group of cyclic nucleotide (Das et al., 2009). The CNBD then undergoes an outward movement, which is evident with P-, B-, and C-helices. In the C-linker domain, the C-helix makes an outward motion, and the A'-helix undergoes an upward (i.e., toward the membrane side) and outward bending, significantly widening the channel pore. The D'-E'-F'-helices of the C-linker remain relatively constant (Gao et al., 2015; Kesters et al.,

2015; Marchesi et al., 2018). The study by Kesters et al., 2015 compared the cryo-EM structure of the cAMP-bound state to that of the cGMP-bound state and found that significant conformational changes are present in the αP-, αB-, and αC-helix of the cAMP-bound state, which move outward compared to the cGMP-bound structure. The binding of cyclic nucleotide to the CNBD stabilizes the outward bend confirmation, which propagates through the C-linker and allows for the proper gating of the channel in response to cyclic nucleotide binding.

The molecular mechanism for the ligand recognition is by the interaction of residues (Table 1.1) in the CNBD with the phosphoribose and the purine ring of the ligand. The alignment of ligands in anti or syn configuration also affects agonistic activity. In the anti-conformation of cGMP, the C-helix of the SthK channel is unable to interact with ligand, which is the reason for cGMP's poor agonistic activity.

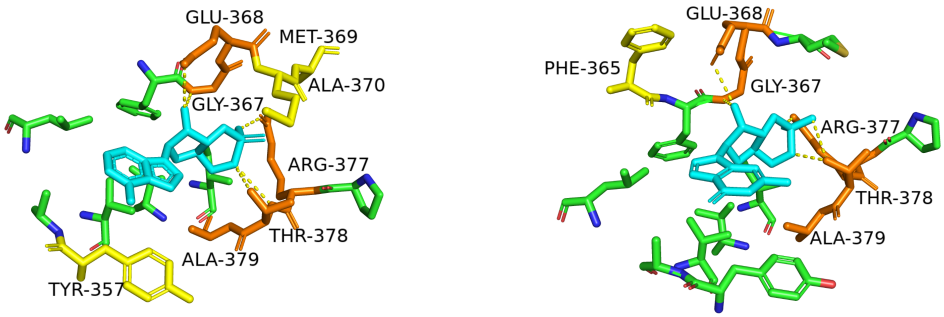

Figure 1.4: Comparison of the amino acids in the ligand binding site involved in recognition of cAMP (left) and cGMP (right) in the SthK channel. Dashed lines represent hydrogen bonds or salt bridges.

1.3.2 Binding Kinetics

The binding kinetics of the SthK channel involves the rapid and specific interactions of the cNMP with the CNBD. The SthK channel exhibits different binding kinetics with cAMP and cGMP. This difference in binding affinity and the structural changes the cNMPs induce upon binding contribute to their varying agonist activity.

Table 1.1: Amino acid residues that interact with cAMP and cGMP in the SthK channel.

cAMP	cGMP
T 378	T 378
R 377	R 377
G 367	G 367
E 368	E 368
A 379	A 379
A 370	F 365
M 369	
Y 357	

Recent analysis with the binding kinetics, the affinity constant, and the structural factors that influence ligand binding revealed that the SthK channel CNBD has a similar association rate constant for both ligands, but the dissociation rate constant of cGMP-CNBD was about twofold higher than that of cAMP-CNBD; that is, cAMP binds around twofold more strongly to the CNBD than cGMP. To delve deeper into the binding mechanism, the team conducted microscale thermophoresis experiments, which showed that H-bond interaction energies with cAMP were larger than those with cGMP, explaining CNBD's higher binding affinity for cAMP. The results obtained from molecular dynamics simulations (MDS) indicate that the CNBD binding pocket can differentiate between cAMP and cGMP by establishing H-bond interactions with Y357 (cAMP) or F365 (cGMP). This interaction results in a strong association of cAMP with the phosphate groups located on the opposite side of the binding pocket, with the involvement of M369 and A370, in line with an earlier study by Kesters et al., 2015 (Table 1.1). Although the structural analysis of CNG channels such as SthK has provided valuable insights into the kinetics and binding of CNs, it remains unclear how amino-acid residues located outside of the binding pocket participate in the opening of the channel and affect the binding of CNs.

1.3.3 Biophysical characterization of SthK

The cAMP-dependent activity of SthK was first demonstrated in patch-clamp recordings of SthK channels expressed in *Xenopus laevis* oocytes (Brams et al., 2014). Multiple studies confirmed the cAMP-dependent activity, whereas only marginal activity was observed in the presence of cGMP (Brams et al., 2014; Morgan et al., 2019; Schmidpeter et al., 2018). A recent study on single-channel bilayer recordings revealed that SthK is differentially regulated by cAMP and cGMP. The efficacy of cGMP is orders of magnitude lower than that of cAMP, even though both ligands display similar binding affinities for SthK (Morgan et al., 2019; Schmidpeter et al., 2018).

The cAMP sensitivity of SthK channels yielded the cAMP concentration of half-maximum activation, EC50 ($K_{1/2}$), of 3.68 ± 0.55 µM and the Hill coefficient (h) of 1.33 ± 0.08 (Brams et al., 2014). A Hill coefficient larger than unity indicates that the subunits cooperate upon channel activation. Of note, while cAMP binding increased channel activity, the maximal open probability in the physiological voltage range and in the presence of saturating concentrations of cAMP is only ~0.1. This means that, on average, only 10 % of the channels are in the open state under these conditions. The SthK channel expressed in *Xenopus laevis* oocyte showed a maximum open probability of 0.13 (Brams et al., 2014) at +100 mV. The open probability strongly increases with depolarization and reaches ~0.7 at +200 mV.

2 Material

2.1 Molecular Biology

2.1.1 HEK293T cell culture

All electrophysiological experiments were carried out on Human Embryonic Kidney cells (HEK293T, ACC 635) purchased from the German Collection of Microorganisms and Cell Cultures (DSMZ, Braunschweig, Germany). The HEK293T cells were cultivated at 37 °C and 5 % CO_2. For better expression to the membrane of HEK cells, the wild-type SthK and the SthK 1.0 mutant were kept at 29 °C and 5 % CO_2 after transfection. The culture was grown using Dulbeccos Modified eagle medium DMEM (Gibco, Thermo Fisher, Germany) with 2 % fetal calf serum (FCS, Biochrom GmbH, Berlin, Germany). No antibiotics or antimycotics were used.

2.1.2 Seeding and transfection of cells

For Patch-Clamp experiments, the cells were seeded in a 4-well multiwell-plate containing PLL-coated 5 mm coverslips (Menzel, VWR, Germany), usually 4-5 coverslips per well. 24 hrs after seeding, the cells were transfected using polyethylenimine (PEI, Merck, Germany). The transfection mixture per well contains 0.8 µg of DNA mixed with 15 µl of Opti-MEM medium and 2 µg of PEI. The mixture was mixed for 10 sec using a vortex mixer and subsequently incubated for 10 minutes at room temperature. Then, the mixture is gently added to the well containing 485 µL of pre-warmed DMEM medium. Finally, 3-5 mM of Sodium butyrate (NaB) is also added to each well. The measurements usually took place 24 hrs to 48 hrs after the transfection.

Table 2.1: Composition of a standard PEI transfection reaction.

Transfection Mixture	**volume**
Plasmid DNA	0.8 µg
OptiMEM	15 µl
PEI	2 µg
NaB	3-5 mM

2.1.3 DNA preparation

All constructs were expressed in HEK cells with the custom-made plasmid pc3Qcit in which the Neomycin resistant gene of the parent plasmid pcDNA (3.1) was replaced by Citrine. All the constructs reported here were designed and integrated into the same plasmid for expression in HEK cells (personal communication Wolfgang Bönigk).

2.1.4 Site-directed mutagenesis

We applied the OE-PCR (overlap extension polymerase chain reaction) method for the site-directed mutagenesis of genes of interest (Fig 2.1). Specific forward and reverse primers were designed and ordered (Eurofins Genomics GmbH, Germany) and combinations of primers were used to run the PCR to generate the desired mutation. To verify the success of the PCR, the products were loaded onto an agarose gel (1 % w/v, Sigma Aldrich, USA). Ethidium bromide (EtBr) was used to stain the probe (Sigma-Aldrich, USA). If DNA bands were detected at the expected positions, the PCR products were cut out, and DNA was extracted using a gel extraction kit (Macherey-Nagel, Germany). Sub-cloned PCR products were sequenced to verify the successful introduction of the mutation (Eurofins Genomics GmbH, Germany). Primers (Table 2.2) were designed according to the regions/residues that needed to be mutated in the gene. The corresponding polymerase chain reaction (PCR) protocol is described in Table 2.5.

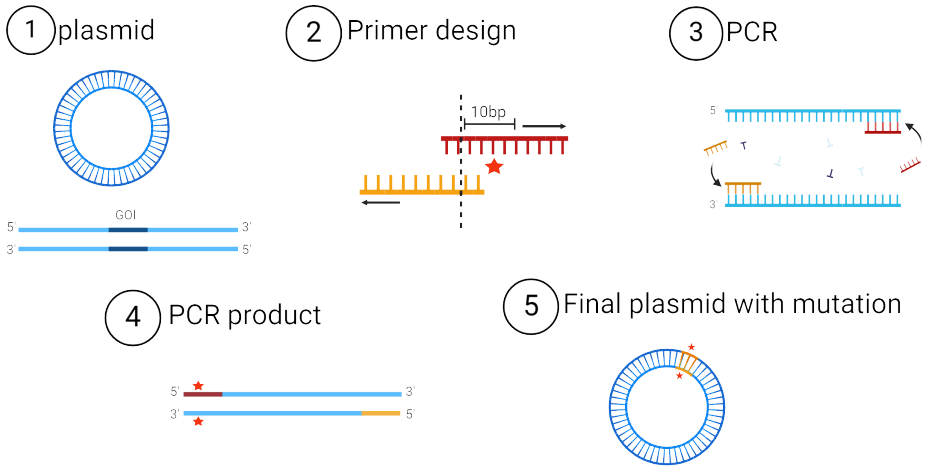

Figure 2.1: Illustration of overlapping PCR for the site-directed mutagenesis.

2.2 Electrophysiology

2.2.1 The Patch-clamp technique

The Patch-clamp technique is a powerful method used to study ion channels in biological membranes with high resolution. In this technique, a small patch of the membrane is electrically isolated by pressing a fire-polished glass capillary (Microelectrode) onto the surface of the cell membrane. By applying a small negative pressure to the pipette interior, a seal of high electrical resistance (tens of gigaohms GΩ) and mechanical stability is formed (Sigworth & Neher, 1980). This seal is commonly referred to as the ”gigaseal”. Currents across this small patch of membrane can then be studied by connecting an electrical amplifier to the patch pipette. The high-resistance of the seal is critical in reducing noise from leak currents across the preparation. With a Gigaohm seal, even single channel currents in the low pA range can be recorded from the isolated area (Neher et al., 1978).

Patch-clamp recordings can be carried out in various configurations, as illustrated in Figure 2.2. To begin, the fire-polished pipette is pressed against the cell membrane, and a gentle suction is applied until the resistance reaches values >1 GΩ. The current can be recorded from the membrane patch while the cell remains intact (Cell-attached). This configuration

Table 2.2: Primer for site-directed mutagenesis.

Primer	Sequence
C1131	5'-TAATACGACTCACTATAGGGAGACCC-3'
C4485	5'-GGATATCCTGGCGGACCTGGCCCTGATTG-3'
C2434	5'-CGGCCTGGTCATTGGTAATATCGC-3'
C2928	5'-TTGTCTAGATTAGACCTTGGCCTTGCTTCTCTTGCG-3'
C4484	5'-CCTATAGGACCGCCTGGACCGGGACTAAC-3'
C2432	5'-ATAGAATTCCCACCATGAAATCGTCCGCCTTCTCCCAC-3'
C2926	5'-CTTGATGGAGGGGTAGCGGCTCAGAATACGATCG-3'
C2927	5'-CTGAGCCGCTACCCCTCCATCAAGGCACAGATC-3'
C2928	5'-TTGTCTAGATTAGACCTTGGCCTTGCTTCTCTTGCG-3'
C3459	5'-GAAATCTTCACCCCAGCCCTTAAACAGCGGG-3'
C3460	5'-GCTGTTTAAGGGCTGGGGTGAAGATTTCATTC-3'
C4348	5'-CCAGGCCGTACATGGCCACACCCAGCAGTTC-3'
C4349	5'-GAACTGCTGGGTGTGGCCATGTACGGCCTGG-3'
C4486	5'-AGACCTTGGCCTTGCTTCTCTTGCGGTCCTTGCTGATTCTCTCTT CAGC-3'

is particularly valuable for studying individual ion channels at a high resolution. The experimenter can study individual channels to understand their conductance, kinetics, and sensitivity to different stimuli. Maintaining a stable Gigaohm seal in Cell-attached Patch-clamp experiments demands precise electrode positioning and controlled environmental conditions.

Once a Gigaohm seal is obtained, the membrane patch can be destroyed by applying rapid, strong suction and/or a strong voltage pulse (>400 mV) in the Cell-attached configuration. This allows the experimenter to gain electrical access to the inside of the cell while maintaining control over the extracellular environment. In this configuration, the current across

Table 2.3: Plasmid and primers involved in generating mutant channels with specific amino acid exchanges.

Mutant channel	Primers used
pc3QCit-SthK-ApCHelix3	C2432 C2926 C2927 C2928
pc3QCit-Sthk 1.0	C2432 C2928 C3459 C3460
pc3QCit-SthK 2.0	C2432 C2928 C4348 C4349
pc3QCit-SthK 1.1 and SthK 2.1	C2432 C2928 C4486

Table 2.4: Standard reaction mixture for a PCR to amplify a gene from a template vector.

PCR reaction mix	volume
pLJ67_flippase	1 µl
2 mM dNTP	5 µl
25 mM $MgSO_4$	2 µl
DMSO	2 µl
KOD Hot Start DNA Polymerase [1 u/µl] (Novagen)	1 µl
Autoclaved ultra-pure water	18 µl
KOD Hot Start DNA Polymerase 10xrxB	5 µl
5 M Betaine	10 µl
Forward primer (5 pmol/µl)	3 µl
Reverse primer (5 pmol/µl)	3 µl

Table 2.5: Standard reaction cycles for the corresponding amplification PCR.

PCR cycles
2 min at 94 °C
35 x [30 sec at 94 °C; 20 sec at 56 °C; 2 min at 68 °C]
2 min final extension at 68 °C

the entire cell membrane can be recorded (Whole-cell), and there is physical access from the patch pipette to the cytoplasmic contents of a cell. The pipette solution replaces the solution inside the cell relatively quickly due to diffusion. This configuration is widely used in electrophysiology to study the macroscopic behavior of ion channels, receptors, and other membrane proteins involved in cellular signaling.

When the pipette in the Cell-attached configuration is quickly withdrawn from the cell, the isolated membrane patch can be removed while the Gigaseal remains intact, resulting in the inside-out configuration. Here, the extracellular side of the membrane faces the pipette solution while the intracellular side faces the bath solution. This versatile configuration allows the experimenter to precisely control the composition of the solution that is perfused onto the cytoplasmic side of the membrane, making it ideal for studying channel modulation and gating by intracellular factors. In contrast, when the pipette is withdrawn slowly from the Whole-cell configuration, an outside-out patch may form by ripping out a small piece of membrane that can then spontaneously close around the pipette, forming a new membrane patch. Now, the extracellular side of the membrane faces the bath solution, while the intracellular side faces the pipette solution. This configuration is useful for studying channel properties influenced by extracellular factors, such as receptor desensitization or drug interaction with channel pores.

In this thesis, all electrophysiological recordings were performed in the voltage-clamp mode. The patch-clamp amplifier is the main component of the electrical circuit. This highly sensitive amplifier can measure Picoampere (pA) current. One pivotal element of

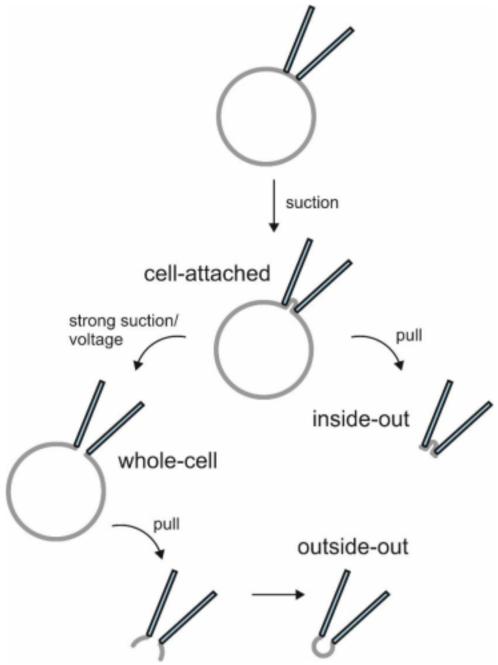

Figure 2.2: Schematic representation of various patch-clamp configurations. After the formation of the gigaseal on the cell (Cell-attached), the pipette can be pulled away to rip out a membrane patch of which the intracellular side faces the bath solution (inside-out). Alternatively, the membrane patch can be destroyed by strong suction or high voltage to gain electrical access to the inside of the cell (Whole-cell). Afterwards, a membrane patch can be excised again where the extracellular side faces the bath solution (outside-out). Modified from Hamill et al., 1981, Courtesy to Wobig, 2021.

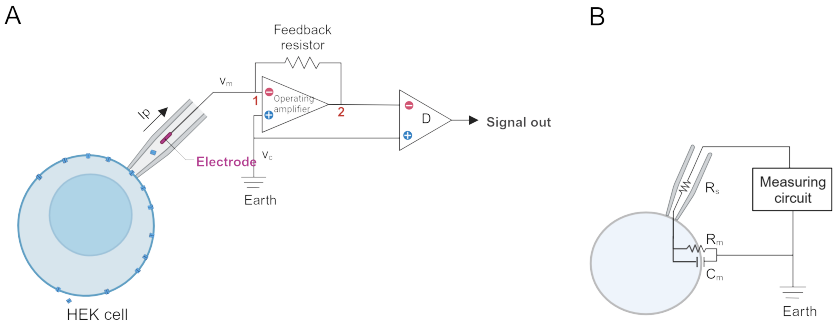

Figure 2.3: Schematic representation of the circuit diagrams in electrophysiology experiments. A: Electric circuit underlying the patch-clamp methodology B: Simplified circuit diagram for the Whole-cell configuration: The cell membrane acts both as a resistor (with resistance R_m), through which currents over the membrane (I_m) flow, and as a capacitor (with capacitance C_m). Additionally, a combination of pipette resistance and access resistance introduces the series resistance (R_s). Adapted from Hamill et al., 1981; Molleman, 2003. Images recreated using BioRender.com.

this circuit is the pre-amplifier located at the head stage. It consists of the operational differential amplifier (op-amp) and the feedback resistance (R_f) (Fig 2.3A). The head stage amplifier is located close to the patch pipette, which helps maintain a high signal-to-noise ratio, which is crucial for accurate measurements. By using the patch-clamp technique, the actual membrane potential (V_m) can be clamped to a desired command potential (V_c) by injecting a current (I). The patch-clamp amplifier achieves this with a feedback amplifier that corrects any changes in voltage and a differential amplifier that measures the required currents (Fig 2.3B). The first amplifier compares the voltage at the pipette (Vm) with the command voltage. V_m is applied at the anode, the V_c at the cathode of the op-amp. As soon as V_m differs to V_c, the op-amp creates a potential at its output V_{out}, which is proportional to the potential difference between V_m and V_c, but amplified with a factor of X

$$V_{\text{out}} = X(V_c - V_m) \tag{2.1}$$

When current is injected over R_f, it causes a voltage drop of

$$V = R_f \times I \tag{2.2}$$

that is measured by the second amplifier (D). In the main amplifier unit, this voltage is converted (using the known value for R_f) back into a current signal (which corresponds to negative I ($-I$)). In this case, a potential difference between points 1 and 2 (Fig 2.3A) exists, and I can flow over R_f:

$$I = \frac{V_{\text{out}}}{R_f} \tag{2.3}$$

Due to high resistance at the op-amp input, the current can only flow through the electrode via the $AgCl_2$ wire to the membrane patch. This adjusts V_m to V_c, effectively clamping V_m to V_c. During the recording, the amplifier compensates for changes in V_m within microsec-

onds. A positive membrane voltage means that the intracellular side of the membrane is charged positively while the extracellular side is charged negatively and *vice versa*. Cations that flow from the intracellular to the extracellular side of the patch constitute an outward current and *vice versa* (Schladt, 2022).

An inverted IX70 microscope (Olympus, Tokyo, Japan) equipped with a 10x or 20x objective was mounted on top of a vibration-dampened table, protected from electromagnetic fields by a Faraday cage. Using two micromanipulators (Scientifica, Uckfield, UK), the recording chamber and the head stage with the patch pipette were moved under the microscope into the field of view. The recording chamber was connected to a gravity-driven perfusion system. A reference electrode ($AgCl_2$) was connected to the solution in the recording chamber via an agar bridge containing 3 M KCl. The pipette solution was electrically coupled to the pre-amplifier via a patch-pipette electrode ($AgCl_2$). Patch pipettes were pulled from 1.5 mm thick borosilicate glass capillaries (Hilgenberg, Malsfeld, Germany) on a DMZ puller (Zeitz Instruments GmbH, Martinsried, Germany) and electrode resistance was 2.5- 5 MΩ for excised patch and 5-10 MΩ for whole-cell recording.

In this thesis, all the patch-clamp experiments are performed in the excised inside-out and Whole-cell configurations to measure channel properties. Excised patches were obtained within seconds to minutes. Holding potentials were 0 for the excised patch and -80 mV for the Whole cell mode. Recordings were performed at room temperature (RT, 22-25 °C) using an Axopatch 200B amplifier (Molecular Devices, Union City, CA, USA), connected to a PC running pClamp 10 (Molecular Devices) via a Digidata 1440A acquisition board. During this thesis, data were filtered with a 10 kHz 4-pole low-pass Bessel filter and digitized with a sampling rate of 25 kHz.

2.2.2 Gravity-driven perfusion system

The solution delivery was via a gravity-driven perfusion system, which utilizes 15 ml syringes connected to a multi-barrel recording chamber by means of transparent silicon tubes

(Fig 2.4A). The flow of solutions was controlled by a 2-way stopcock with luer locks and influenced by gravity. The tubes were designed to be leak-proof to prevent air bubbles from obstructing the flow. Once the inside-out patch was obtained, the pipette tip was precisely directed and placed into the recording chamber barrel (Fig 2.4B) using a micromanipulator (Fig 2.4C). The reservoir valve was then turned on to expose the ion channel present on the patch to varying concentrations of cyclic nucleotide in order to obtain macroscopic current.

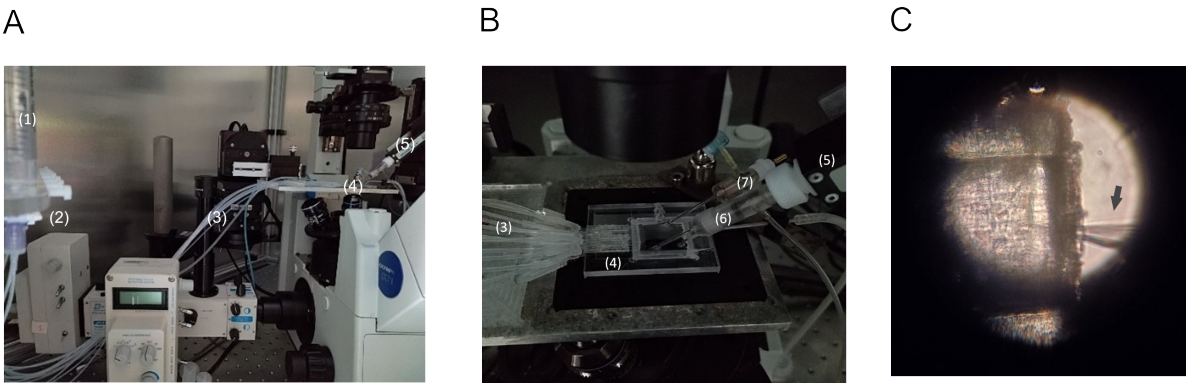

Figure 2.4: Gravity-driven perfusion system. Photographs with its components (a). Enlarged view of recording camber (b) and enlarged view of the pipette tip in the solution outlet tube end. (c). The labeled items in the photographs refer to (1) syringe, (2) valves, (3) tubes, (4) recording chamber, (5) headstage, (6) pipette holder, and (7) bath electrode with agar bridge.

2.2.3 The liquid-junction potential

When two solutions with varying ionic compositions come into contact at an interface, an ionic potential arises from differences in ion concentration and mobility between the two solutions. In electrophysiology, this ionic potential is called liquid-junction potential (LJP). LJP occurs due to the difference in electrolytes of the intracellular solution inside the patch-pipette and the extracellular bath solution. For instance, the pipette solution might lose K^+ faster than gaining Na^+ ions and gain Cl^- ions more rapidly than losing Asp^-. However, once the Gigaseal is established, the pipette solution is no longer in contact with the bath

solution, and the LJP disappears. Throughout the subsequent measurement, if the offset potential is not corrected, it will be added to the membrane potential, leading to an error in the applied membrane voltage. Researchers employ a technique called LJP compensation to counteract this error. To mitigate the influence of LJP on voltage measurements, I used the liquid-junction potential calculator JPCalcW in this thesis. This program, included in the pClamp 10 software, is based on the JPCalc software program by Barry, 1994. The liquid-junction potential for ES and IS was 15.26 mV, and the membrane voltage was adjusted accordingly offline.

2.2.4 Solutions for recording

Table 2.6: Composition of the ES solution.

Chemicals	**Concentration**
NaCl	140 mM
KCl	5.4 mM
$CaCl_2$	1.8 mM
$MgCl_2$	1 mM
Glucose	10 mM
HEPES	5 mM
pH (adjusted with NaOH)	7.4
Osmolarity	298 mOsm

2.2.5 Data analysis and illustrations

Data analysis was done using Clampex 10.7.0.3 software (Molecular Devices) and curve fitting was performed with Origin 9.0 (OriginLab Corp.). Images were processed and analyzed using Fiji (ImageJ) version 1.54f (Schindelin et al., 2012). The figures were made using OriginPro 9.0, Inkscape 1.3.2 and the channel protein structure was created with PyMOL(TM) 1.7.6.2. The illustrations were created using BioRender.com.

Table 2.7: Composition of the IS solution.

Chemicals	Concentration
NaCl	10 mM
Potassium aspartate (KAsp)	130 mM
EGTA	1 mM
$MgCl_2$	2 mM
HEPES	10 mM
Na2ATP	2 mM
pH (adjusted with KOH)	7.4
Osmolarity	260-280 mOsm

Table 2.8: Composition of the High KCl solution for excised inside-out recordings.

Chemicals	Concentration
KCl	145 mM
HEPES	5 mM
EGTA	2 mM
pH (adjusted with KOH)	7.4

2.3 *Ex vivo* study

2.3.1 AAV-Virus injections

30 minutes before surgery started, mice received an intraperitoneal injection of buprenorphine (0.05 mg/kg body weight), and all surgical equipment and surfaces were cleaned with 70 % ethanol. Anesthesia was induced using 3.5 % isoflurane mixed with 20 % oxygen in an induction chamber. After mice were deeply anaesthetized, they were transferred into a stereotactic frame (Kopf instruments), fixed by putting the front teeth into the mouth holder and pointy ear bars in the ear channels, and anesthesia was maintained using 1.1 – 1.3 % isoflurane. Eye ointment (Bepantene) was applied on both eyes and the scalp disinfected

with iodine solution (Betaisodouna, Mundi Pharma) and a local anesthetic (10 % lidocaine) was applied. The scalp was well shaved using scissors and if necessary thoroughly de-haired using an electric nose hair trimmer. Next, a small incision of the scalp was made using scissors and the underlying tissue cleaned with a cotton swap, until the bone sutures were well visible. Using the tip of the injection needle, the proper alignment of the skull marks “bregma” and “lambda” were checked for in the medial-lateral orientation, corrected by adjusting the ear bars if necessary. To ensure proper antero-posterior alignment, the height difference between lambda and bregma was corrected and extra care was taken to ensure that the variation did not exceed 0.05 mm. After successful alignment, the injection coordinates were marked on the skull using a waterproof pencil and a drill hole was made with a small drill bit (FINE SCIENCE Tools). Prior to entering the brain with the needle, a small test injection of a small amount of liquid was made into the air to assure proper virus outflow of the syringe. The needle was then inserted into the brain and slowly brought into position by lowering it into the brain. For injection into the CA1 regions, 500 nL per hemisphere of an adeno-associated virus **pAAV-Syn-EYFPTr64 CaRhGC-T2A-SthK 2.1** (Fig 3.10C) generated in the lab was injected into C57BL6/N mice of both genders aged between 18-24 weeks used via a nanofill syringe (World Precision Instruments) at a speed of 100 nL / min using the following coordinates: AP 1.9, ML +/- 1.6 and DV 1.6. When the virus was injected at DV 1.6, the needle was slowly withdrawn 5 minutes after the end of the virus infusion. After removal from the brain, a small test injection of 50 nL of the virus was made into the air to ensure proper virus outflow. Lastly, the incision into the scalp was sutured with 3 or 4 stitches using absorbable surgical silk (VICRYL Plus, Ethicon, Germany). Animals were given 5 mg /kg bodyweight Ketoprofen (Gabrilen, Tommdorff, Germany) subcutaneously at the end of the surgery and for post-op care 24, 48 and 72 hrs after surgery.

2.3.2 Perfusion of animals

Transcardial perfusion was performed to preserve the integrity of the brain tissue. Mice were anaesthetized by I.P (intraperitoneal injections) of Ketamin (100 mg/kg) and Xylazin (16 mg/kg) i.e 0.1 ml/10 g of body weight. After assessment of lack of pain reflexes (toe and tail pinch), mice were transcardially perfused with cold phosphate-buffered saline (PBS), followed by 4 % Formaldehyde (FA). Afterwards, the brain was removed and placed in 4 % FA at 4 °C overnight.

2.3.3 Immunohistochemistry

Coronal brain slices, 50 µm thick, were cut in sequential order from the rostral to the caudal area using a vibratome (HM650V, MICROM Germany). Slices with hippocampus sections were collected and washed in PBS (Phoshate Buffered Saline), blocked in 10 % normal goat serum (NGS) and 0.25 % TBS-T (Tris-buffered Saline with Triton-X-100) for 2 hours at room temperature, and transferred to the primary antibody solution (primary antibody in 5 % NGS/ 0.1 % TBS-T) for 4 °C overnight. For GFAP staining, an additional antigen retrieval step was performed by keeping the slices in citrate buffer at 60 °C overnight. The slices were then washed with TBS and transferred to the same primary antibody solution.

Table 2.9: Primary and secondary antibody incubation buffer.

Antibody solution	**Steps**
Primary antibody solution	1. TBS-T 0.1% 2. NGS 5 % 3. Primary antibodies (1: 500)
Secondary antibody solution	1. TBS 2. Secondary antibodies (1: 1000)

The primary antibodies used in our protocol were

1. anti-GFAP monoclonal rabbit antibody (Abcam ab68428) at a dilution of 1:500,
2. anti-NeuN polyclonal chicken antibody (Synaptic Systems 266006) at a dilution of 1:500

Next, slices were washed in TBS and transferred into the secondary antibody solution (secondary antibody in TBS) for 2 hours. Secondary antibodies used were

1. Goat anti-chicken Alexa 555 (Invitrogen A21437) at a dilution of 1:1000
2. Goat anti-rabbit Alexa 647 (Invitrogen A21245) at a dilution of 1:1000.

Finally, slices were stained with 4,6 Diaidino-2-phenylindole (DAPI) for 30 min at room temperature at a dilution of 1:1000. Then, slices were washed in PBS and mounted on glass slides with mounting media (Aqua Poly/Mount, Polysciences, Warrington, USA). Glass coverslips were carefully fixed to avoid trapping air bubbles and left undisturbed to dry overnight.

2.3.4 Confocal Imaging

Image acquisition was done using a confocal microscope (Stellaris, Leica Microsystems). For overview pictures, we employed a 10x magnification dry objective (numerical aperture, 0.4) and a 512 x 512-pixel resolution (pixel size, 0.002 mm). To investigate the number and morphology of neurons and astrocytes in the CA1 region, we employed a 20x magnification objective (numerical aperture, 0.75), a 1024 x 1024 pixel resolution (pixel size, 0.001 mm), and acquired images. In total, I imaged 3 slices per mouse. We used images obtained from a 20x magnification objective to investigate the width of the *stratum pyramidale* and chronic astrogliosis. Tiled fluorescent images of the brain sections covering the hippocampus were taken. We measured the relative expression intensities of GFAP labelling in the virus-expressing dorsal CA1 at three positions along the anteroposterior axis. The quantification was performed in Fiji ImageJ by drawing 3 square-shaped regions of interest

(ROI) around GFAP expression in CA1 (*stratum oriens* to *stratum radiatum*) and taking the mean grey area of the GFAP labelling within this ROI. Areas with glial scarring around the injection point were excluded by adjusting the ROI. The same measurement was done in the contralateral CA1 (GFP) by drawing a similar ROI. For normalization, in each slice, the local background was measured in a small square in the cortex and subtracted from the mean grey areas of each ROI in CA1. In addition, to determine the width of the pyramidal cell layer in the dorsal medial CA1, we measured four perpendicular lines in both the left and right CA1 of each NeuN-labeled section. We then compared the average width of the pyramidal cell layer in the left and right CA1.

3 Result

3.1 Ion channel

3.1.1 SthK C-Helix

The main task of my thesis was to switch the ligand selectivity of the SthK channel. It has been reported that the C-helix segment within the CNBD plays a significant role in the ligand selectivity of CNG channels (Gordon & Zagotta, 1995b; Goulding et al., 1994). I replaced the C-helix region of the Wt SthK channel with that of a highly cGMP-sensitive K^+ selective CNG channel (CNGK) found in the sperm of the sea urchin *A. punctulata* (Fig 3.1 A). The CNGK channel operates at nM range of cGMP while being 500 times less sensitive to cAMP. This CNGK channel has a pseudo-tetrameric structure, with the CNBD of the third repeat being the reason for its cyclic nucleotide selectivity and sensitivity (Bönigk et al., 2009). The chimeric SthK channel with the replaced C-helix region from the third repeat of the CNGK channel was named SthK ApCHelix3 (SthK C-Helix) (Fig 3.1B).

I transfected the plasmid of the mutant channel into HEK293T cells. After 48 hrs of transfection, I conducted electrophysiological experiments to characterize this channel. The channel was functionally expressed onto the cell membrane. Mostly, the excised inside-out patches contained only few channels. When exposed to saturating concentrations of cGMP and cAMP, the currents were larger for cAMP than for cGMP. Fig 3.2A shows an excised inside-out patch with 3 channels recorded at -50 mV, displaying a larger current with saturating concentration cAMP than with saturating cGMP. I calculated the ratio of currents, activated by saturating concentrations of cGMP by those activated by saturating concentrations of cAMP; this value is called fractional activation in the CNG channel. I ob-

served an average value of 0.245 (Fig 3.2B) for the SthK C-Helix channel. Next, I studied the open probability (Po) of the mutant channel. To estimate Po, I fitted the all-point amplitude histogram using Gaussian curves and estimated the single channel Po by binomial distribution fitting (see for example Fig 3.2C and Fig 3.2D). At -50 mV, the mutant channel showed a mean value Po of 0.16 ± 0.03 (n=4) for 1 mM cAMP and 0.04 ± 0.03 (n=4) for 1 mM cGMP. The previously reported Po of the Wt SthK channel for saturating cAMP is 0.14 at +100 mV and 0.65 at +200 mV, according to Brams et al., 2014 and Kuo et al., 2007.

A

```
CNGK 3rdCNBD      GKGRFFGEISLVFSCPRTASIRAENNVDMFVLTKEDLDEVLTHYPSIKAQIYTVAEERISAVRKRSKAKV
SthK              SEGQFFGEMALILRAPRTATVRARTFCDLYRLDKETFDRILSRYPEIAAQIQELAVRRKEELEGGTSRRG
SthK C-Helix      SEGQFFGEMALILRAPRTATVRARTFCDLYRLDKETFDRILSRYPSIKAQIYTVAEERISAVRKRSKAKV
                  *********************************************.* ***  :*  * .
```

B

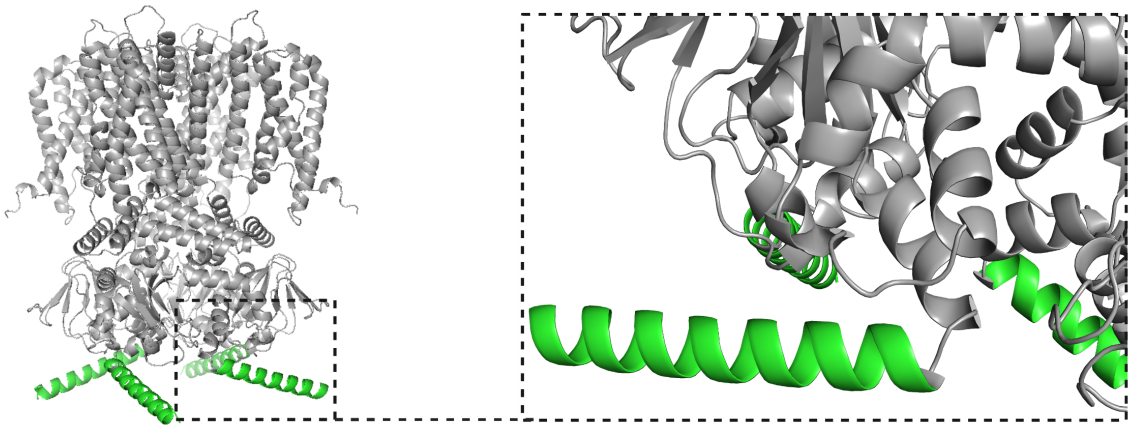

Figure 3.1: SthKApCHelix3 channel (SthK C-Helix). A, Sequence comparison of the Wt SthK (black) and the CNGK channel (red) with that of the mutant channel; the replaced residues in the sequence are shown in green. B, Cartoon representation of the SthK channel with replaced C-helix region (green).

To determine the dose-response relation, I measured the macroscopic current at various concentrations of cAMP perfused to the patch, while recording the steady state current at -50 mV. I fitted the Hill equation to the data to find the concentration of half-maximal activation ($K_{1/2}$) and the Hill coefficient (h). The mutant channel yielded a $K_{1/2}$ of 2.91 µM and a Hill coefficient of 1.03 (n=8) (Fig 3.2E). This indicates that the efficacy for cAMP remained consistent compared to the wild-type SthK, which had a $K_{1/2}$ of 3.7 µM and an

h of 1.3, as reported in *Xenopus oocytes* (Brams et al., 2014). I was unable to determine the cGMP dependence for this mutant. Compared to the wild-type SthK, the SthK C-Helix channel showed an increase in efficacy for cGMP, but with a low open probability. Nonetheless, it appeared to be a promising candidate for further mutations to improve its properties.

3.1.2 Improving ligand selectivity and efficacy

The next task was to enhance the potency of cGMP and decrease the agonistic activity of cAMP. I induced point mutations by altering amino acids within the CNBD region and the C-helix region. First, to increase the agonistic activity of cGMP, Threonine 378 was replaced by Serine (Fig 3.3). This amino acid exchange was inspired by a study in the rod CNG channel that reported a 5-6 fold increase in cGMP activation, when the respective Threonine 560 was exchanged to Serine (Altenhofen et al., 1991). Secondly, to reduce the agonistic activity of cAMP, I replaced Valine 422 with Aspartate (Fig 3.3). A study on the bovine rod CNG channel found that Aspartate at the respective position (604) has a repulsive effect on cAMP (Varnum et al., 1995). Third, to improve the efficacy of the channel for ligands, Alanine 305 was replaced with Tryptophan (Fig 3.3). A Tryptophan at the respective position in the rat olfactory channel was shown to enhance the efficacy of channel activation (Rich et al., 2001).

I added these 3 point mutations to the SthK ApCHelix3 channel, the resulting mutant will be named SthK 1.0 for the rest of the text. 24-48 hrs post-transfection, the channel functionally expressed to the membrane of the cells. Measuring in the whole cell configuration with a pipette solution containing 10 µM of cGMP showed a large outward current (Fig 3.4A, upper) but not in the absence of cGMP (Fig 3.4A, lower). Perfusing an excised inside-out patch with 3 channels with saturating concentrations of cAMP and cGMP shows higher channel opening for cGMP compared with cAMP (Fig 3.4B). I determined the open probability of this channel at saturating concentration of cAMP and cGMP (see for example,

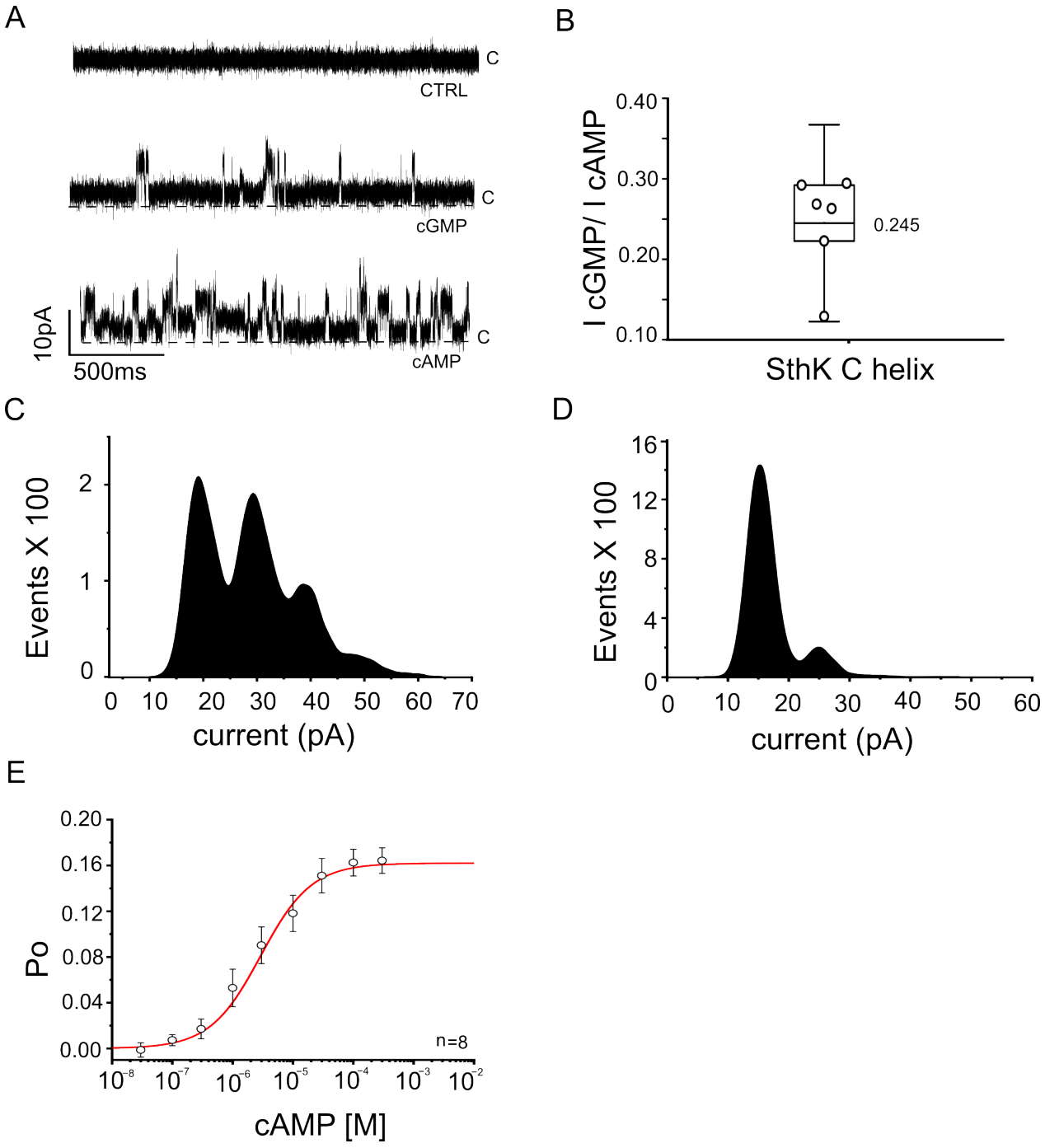

Figure 3.2: Biophysical Characterization of the SthKApCHelix3 channel (SthK C-Helix). A, Representative 3 channel recording traces from SthK C-Helix at -50 mV in the absence of cNMP (top), with cGMP (1 mM, middle) and cAMP (1 mM, bottom). B, The fractional activation I cGMP/I cAMP (± S.D.) is 0.245. C, D, All-point amplitude histograms obtained from 5 channels inside-out patch at -50 mV. Po is 0.18 at 1 mM cAMP (C) and 0.03 at 1 mM cGMP (D). E, Dose-response curve for cAMP normalized to the mean Po. The solid black line represents fit of the Hill equation with $K_{1/2}$ = 2.91 μM and h = 1.03 for 8 patches. Points and error bars represent mean ± S.D.

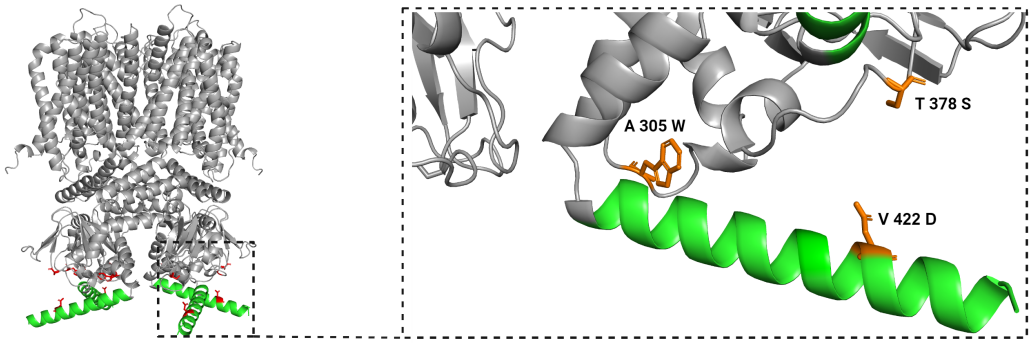

Figure 3.3: SthK ApCHelix3 WSD mutant channel (SthK 1.0). Cartoon representation of the SthK ApCHelix3 WSD channel, the three mutated residues are shown as orange sticks.

Fig 3.4C and Fig 3.4D). The mutant channel showed a mean Po of 0.10 ± 0.03 (n=3) for 1 mM cGMP and 0.04 ± 0.005 (n=3) for 1 mM cAMP. Notably, the cGMP efficacy improved significantly while that of cAMP is reduced (Fig 3.4E). In order to check the efficacy for ligands, I obtained the dose response relation and calculated $K_{1/2}$ value and the Hill coefficient (h). The $K_{1/2}$ value for cGMP is 1.79 µM with h = 1.69 (n=10), while $K_{1/2}$ value for cAMP is 36.49 µM with h = 1.14 (n=3) (Fig. 3.4F).

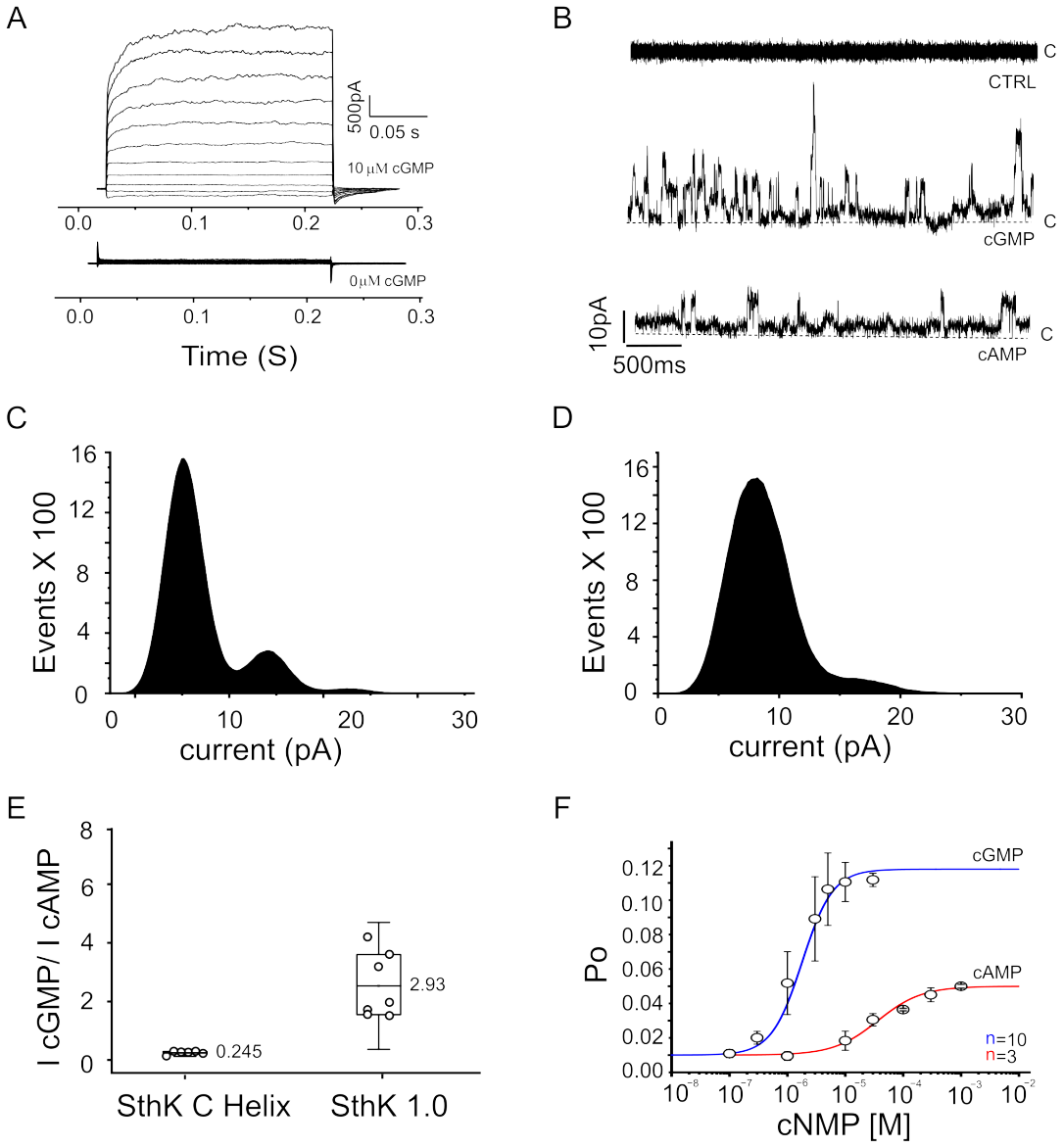

Figure 3.4: Biophysical Characterization of the SthK ApCHelix3 WSD mutant channel (SthK 1.0). A, Whole cell recording of an HEK293T cell expressing the mutant channel, without ligand (bottom) and with 10 µM cGMP in the pipette (top), B, Representative 3-channel recording in the absence of cNMP (top) and the presence of 1mM cGMP (middle) and 1 mM cAMP (bottom). C, D, All-point amplitude histograms from a 2 channel inside-out patch at -50 mV. Po is 0.05 at 1 mM cGMP (C) and 0.02 at 1 mM cAMP (D). E, The fractional activation I cGMP/I cAMP (± S.D.) is 2.93. F, The dose response relation with the ligands against open probability at 50 mV. Solid line represents fit of the Hill equation with cGMP (blue) $K_{1/2}$ = 1.79 µM with h = 1.69, and cAMP (red) $K_{1/2}$ = 36.49 µM with h =1.14. Points and error bars represent mean ± S.D for n patches.

3.1.3 Further improvements to increase the open probability

The SthK 1.0 mutant channel had a moderate open probability, making it inefficient for optogenetic tool development. Therefore, I wanted to enhance the channel's maximum open probability. I induced two point mutations at the C-linker region by replacing Arginine 284 and Glutamate 290 with Glutamine (Q) to improve the gating properties (Fig 3.5). These mutations are inspired by a study comparing the rod CNG channel and TAX-4 channel, where researchers identified important amino acids in the C-linker region that affected efficacy (Paoletti et al., 1999). To further improve the open probability, I induced a point mutation at the S6 domain, where I substituted Alanine 208 with Valine (V) (Fig 3.5). A study carried out on the wild-type SthK channel demonstrated that this mutation results in a higher maximal open probability (Morgan et al., 2019).

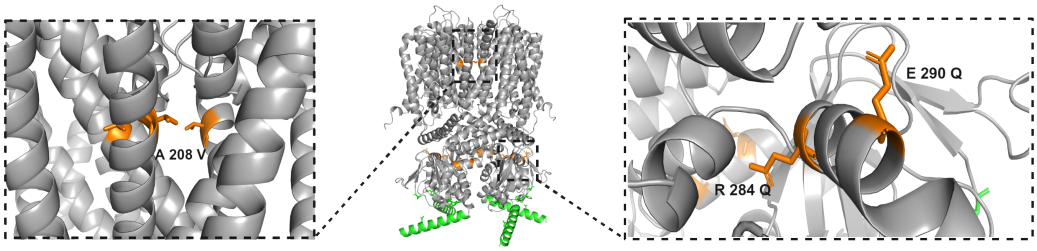

Figure 3.5: Key amino acid exchanges to obtain the mutant channel SthK 2.0. Cartoon representation of the SthK 2.0 channel, the three additionally mutated residues are shown as orange sticks.

These three mutations were added to the SthK 1.0 channel background. The resulting mutant channel was named SthK ApCHelix3 WSD VQQ (SthK 2.0). I transfected the plasmid into HEK293T cells. After 24 hours, the channels displayed high expression on the membrane of the cells. A recording in whole-cell configuration mode from a cell with mutant channels expressed revealed a large outward current in the presence of 100 µM cGMP (Fig.3.6A, top) and no outward current in the absence of cGMP (Fig.3.6A, bottom). Perfusing an excised inside-out patch containing 15 channels with 1 mM cGMP or 1 mM cAMP

showed a larger current in cGMP with stable channel gating for both cyclic nucleotides (Fig 3.6B). An all-point amplitude histogram analysis using saturating concentrations of ligands (see for example Fig 3.6C and Fig 3.6D) results in the mean maximum open probability of 0.35 ± 0.02 (n=3) for 1 mM cGMP and 0.24 ± 0.02 (n=3) for 1 mM cAMP at -50 mV. Of note, the fractional activation by cGMP relative to cAMP at -50 mV reduced from 2.93 in the SthK 1.0 to 1.46 in this mutant (Fig 3.6E). Further characterization using the dose-response relation revealed that the cGMP agonistic activity had increased, the $K_{1/2}$ value was 220 nM with h= 1.87 (n=5), while for cAMP, it was $K_{1/2}$ =14.56 μM with h= 1.58 (n=6) (Fig 3.6F).

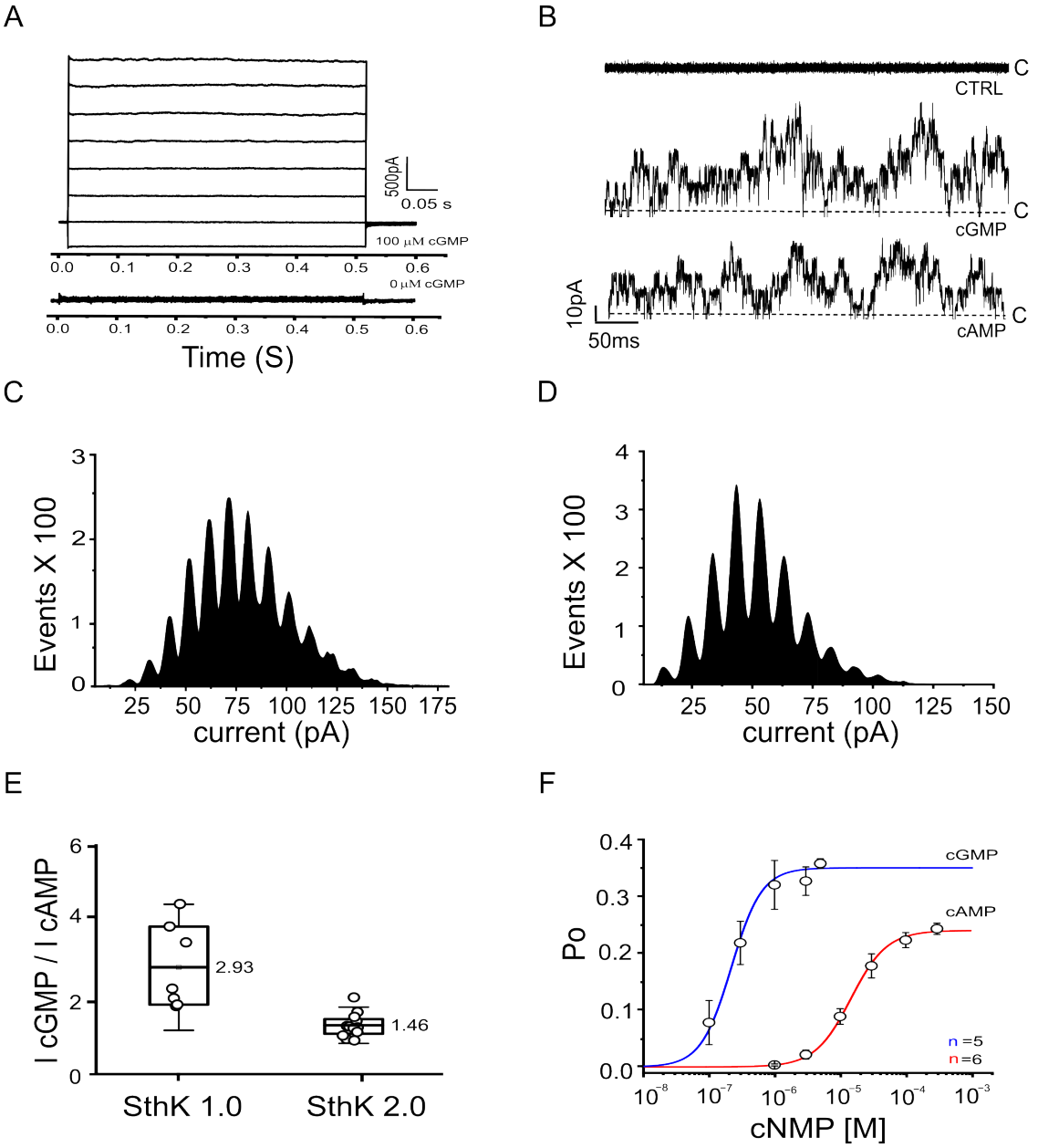

Figure 3.6: Biophysical Characterization of the SthK 2.0 channel. A, Whole-cell recording of an HEK293T cell expressing the mutant channel with 100 µM cGMP in the pipette (top) and without ligand (bottom). B, Representative 15-channel recording in the absence of cNMP (top) and in the presence of 1 mM cGMP (middle) and 1 mM cAMP (bottom). C, D, All-point amplitude histograms from a 15 channel excised inside-out patch at -50 mV. Po is 0.32 at 1 mM cGMP (C) and 0.26 at 1 mM cAMP (D). E, The fractional activation of the channel at cGMP (1 mM) relative to that at cAMP (1 mM) (at -50 mV) is 2.93 for SthK 1.0 (n=7) and 1.45 for SthK 2.0 (n = 12). Line represent the mean value and error bars represent S.D. F, Dose-response relation at -50 mV. Solid line represents a fit of the Hill equation with $K_{1/2}$ cGMP = 0.219 µM with h = 1.87 (blue), and $K_{1/2}$ cAMP = 14.56 µM with h =1.58 (red). Points and error bars represent mean ± S.D for n patches.

3.1.4 C-Helix Mutant A421K

To minimize potential side effects from endogenous cAMP signaling, I tried to further increase the discriminatory potency of the candidate channel to select cGMP. A Cryo-EM structural study of the TAX-4 channel from *C. elegans* showed that Lysine at position 619 interacts uniquely with cGMP rather than cAMP (Fig 3.7A). This may be the reason for its predominant cGMP selectivity, as suggested by the group's findings (Li et al., 2017). In the SthK channel, the representative position for Lysine 619 is Alanine 421 (as shown in Fig 3.7B). I replaced Alanine 421 with Lysine in both, SthK 1.0 and SthK 2.0 (Fig 3.7B), yielding the SthK 1.1 and SthK 2.1 channels, respectively.

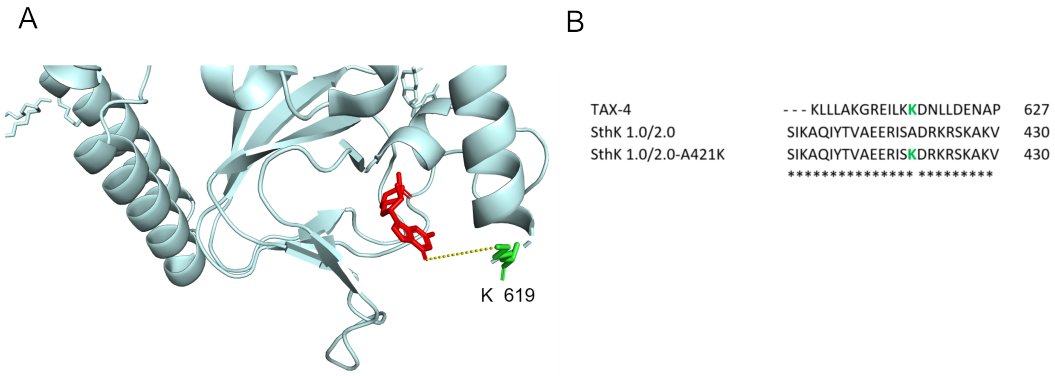

Figure 3.7: SthK ApCHelix3 WSD A421K channel (SthK 1.1). A, Cartoon representation of the interaction of cGMP and the Lysine residue in the TAX-4 channel, Lysine 619 (shown as green sticks) interacts with cGMP (red). B, Sequence comparison of TAX-4 (top), SthK 1.0 and 2.0 (black), the replaced residue (green) in the 421K mutant channel sequence.

24-48 hrs post-transfection, the channels expressed to the membrane of the HEK293T cells. First, I analyzed the SthK 1.1 channel. The excised inside-out patch with 9 channel patch perfused with saturating concentration of ligand showed a larger current with cGMP than cAMP (Fig 3.8A); I calculated the fractional activation by cGMP relative to cAMP ($I_{cGMP/IcAMP}$) to be 15.13 (n=15) whereas in the parent SthK 1.0, the value is 2.93 (n=7) (Fig 3.8B). The $I_{cGMP/IcAMP}$ value has increased fivefold.

Next, I analyzed the open probability using an all-point amplitude histogram (see for ex-

ample Fig 3.8C and Fig 3.8D) and found that for saturating cGMP, mean Po was 0.18 ± 0.04 (n=3) and for saturating cAMP, it was 0.01 ± 0.003 (n=3). To check the efficacy, I plotted the dose-response relation of the mutant channel with ligands and calculated the $K_{1/2}$ value. The concentrations for half-maximal activation for cGMP and cAMP are 3.71 μM with h = 1.74 (n=5) and 48.79 μM with h = 1.24 (n=4) (Fig 3.8E), respectively.

I also tested and characterized the A421K mutation in the SthK 2.0 background. The resulting SthK 2.1 channel also expressed well to the cell membrane (Fig 3.9A). It is noteworthy that the fractional activation value has increased to 1.76, compared to the parent channel of 1.46, as shown in Figure 3.9B. The cGMP discriminative power has improved compared to the parent channel. The mean maximum open probability (see for example Fig 3.9C and Fig 3.9D) was 0.40 ± 0.04 (n=4) for 1 mM cGMP and 0.22 ± 0.05 (n=4) for 1 mM cAMP. The concentrations for half-maximal activation for cGMP and cAMP are 0.66 μM with h =1.59 (n=4) and 18.16 μM with h=1.32 (n=4) respectively (Fig 3.9E). The ability of the channels with the A421K mutation to discriminate between cGMP and cAMP is enhanced compared to that of the respective parent constructs.

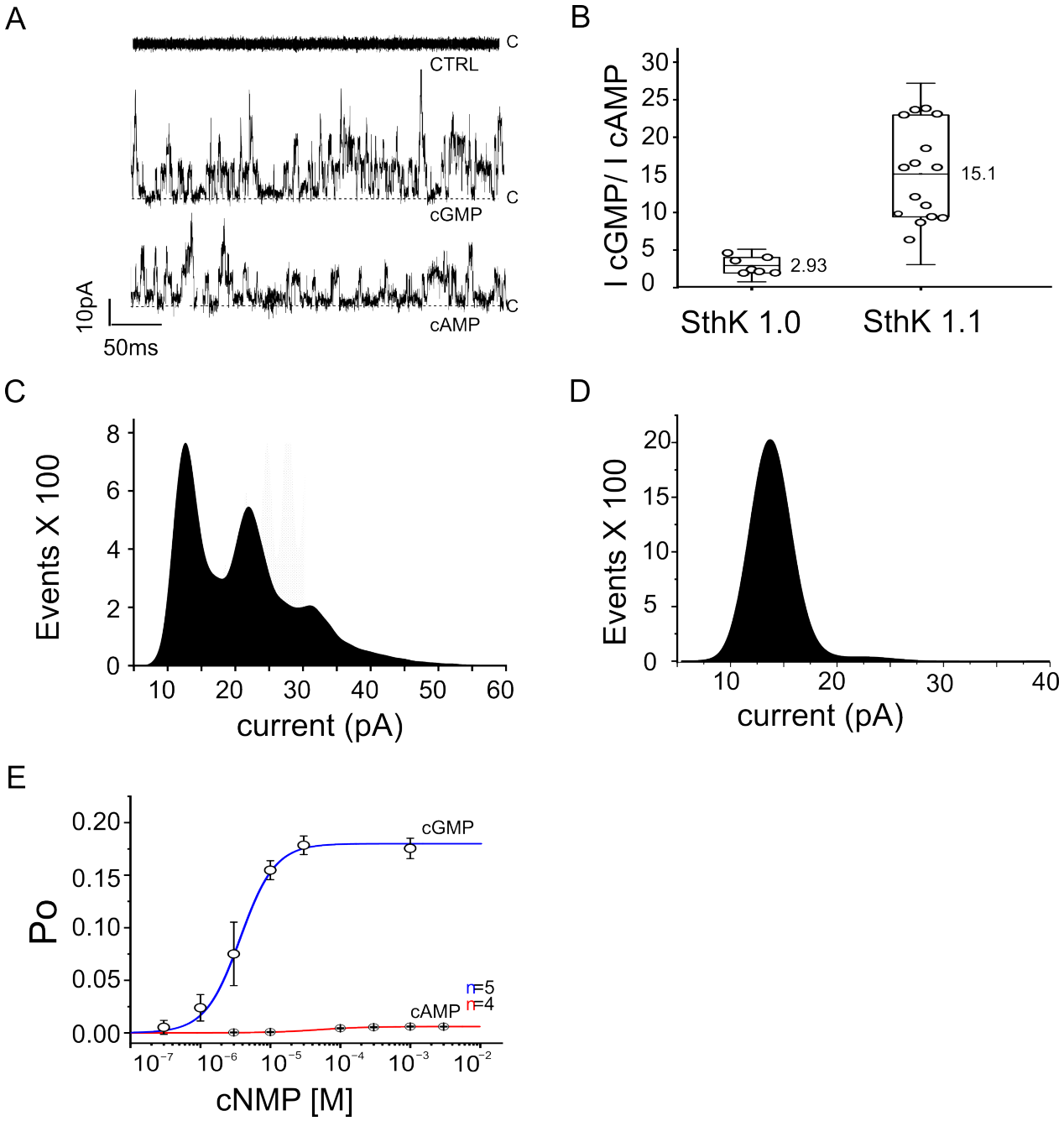

Figure 3.8: Biophysical characterization of the SthK 1.1 channel. A, Representative 9 channel recording in the absence of cNMP and in the presence of 1 mM cGMP (middle) and 1 mM cAMP (bottom). B, The fractional activation by 1 mM cGMP relative to 1 mM cAMP at -50 mV is 2.93 (n=7) for SthK 1.0 and 15.13 (n = 15) for SthK 1.1. Line represent the mean value and error bars represent the S.D. C, D, All-point amplitude histograms from a 4-channel inside-out patch at -50 mV. Po is 0.18 for 1 mM cGMP (C) and 0.016 for 1 mM cAMP (D). E, Dose-response relation with the ligands against open probability at 50 mV. Solid line represents fit of the Hill equation with $K_{1/2}$ cGMP = 3.71 μM with h = 1.74 (n=5, blue), and $K_{1/2}$ cAMP = 48.79 μM with h = 1.24 (n=4, red). Points and error bars represent mean ± S.D for n patches.

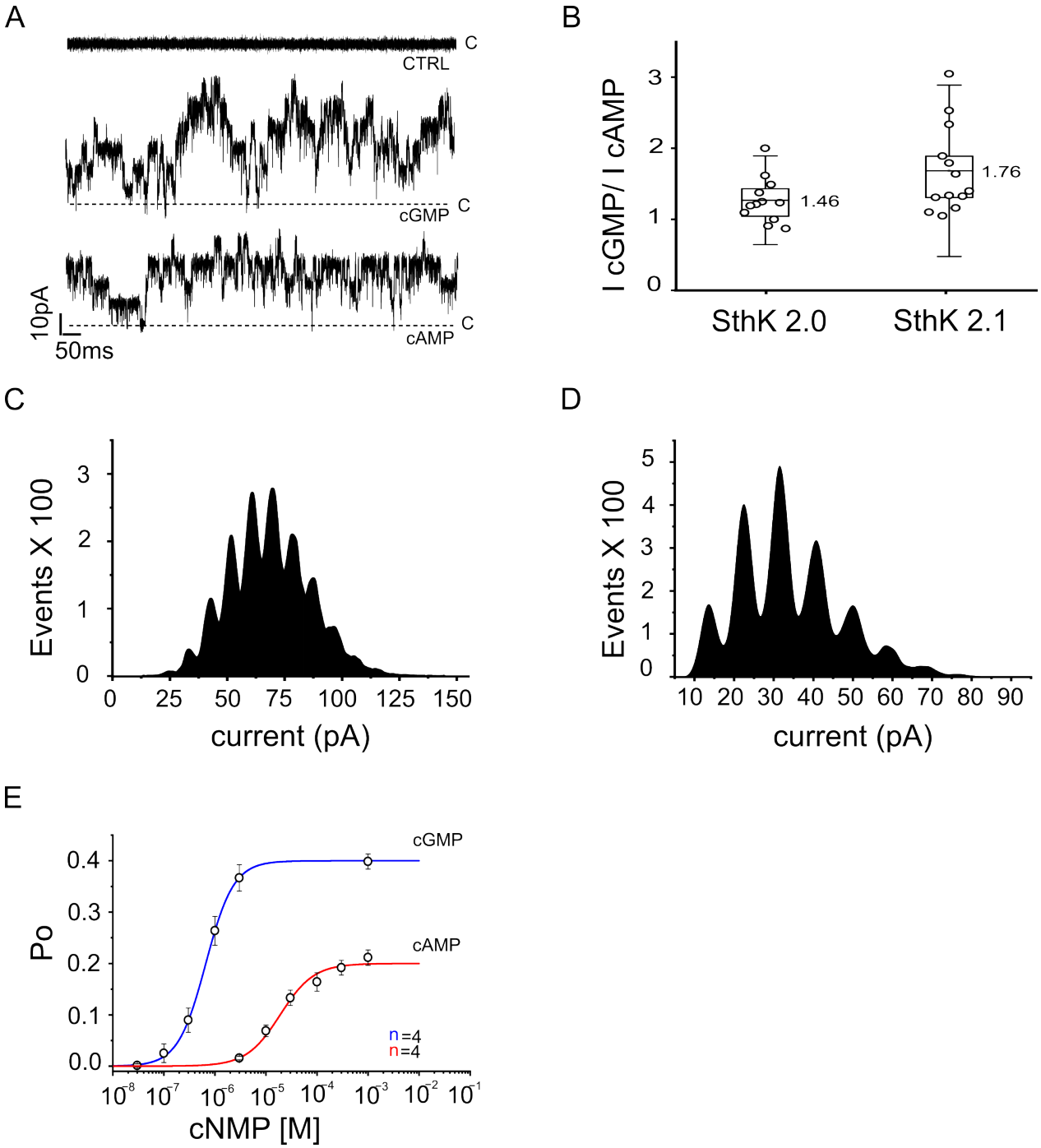

Figure 3.9: Biophysical Characterization of the SthK 2.1 channel. A, Representative 12-channel recording in the absence of cNMP (top) and in the presence of cGMP (1 mM) (middle) or cAMP (1 mM) (bottom). B, The fractional activation of the channel at 1 mM cGMP relative to 1 mM cAMP (at -50 mV) is 1.46 (n=12) for SthK 2.0 and 1.76 (n = 13) for SthK 2.1, the line represents the mean value and error bars represent the S.D. C, D, All-point amplitude histograms from a 9-channel inside-out patch at -50 mV. Po is 0.34 for 1 mM cGMP (C) and 0.19 for 1 mM cAMP (D). E, Dose-response relation with the ligands against open probability at -50 mV. Solid line represents a fit of the Hill equation with $K_{1/2}$ cGMP = 0.66 μM with h = 1.59 (n=4, blue), and $K_{1/2}$ cAMP = 18.96 μM with h = 1.32 (n = 4, red). Points and error bars represent mean ± S.D for n patches.

3.2 Functional expression of RoCK 2.1 and histological changes in long-term use *in-vivo*

After careful consideration, we have chosen the SthK 2.1 channel as the candidate channel for RoCK 2.1. Our next step is to evaluate the effectiveness of this tool in different systems, including a neuronal-like cell line and cultured hippocampal neurons. These experiments were performed by our Berlin coworkers Anika Spreen and Yinth Bernal Sierra. We first expressed RoCK 2.1 in ND7/23 cells. Co-expression was performed with the SthK 2.1 channel and an N-terminally truncated Rhodopsin Guanylyl Cyclase (tr64_CaRhGC) in a single vector, separated by a protein splicing spacer T2A (YFP-CaRhGC-T2A-SthK 2.1 (Fig 3.10A). We conducted a light titration curve analysis on ND7/23 cells that expressed RoCK 2.1. The result shows an intensity-dependent outward current activated by 525 nm light, as shown in Figure 3.10B. Notably, with the SthK 2.1 channel, RocK 2.1 demonstrated high sensitivity to light, with a half-saturation value of 1.1 mW/mm2. Next, we evaluated the performance and efficacy of RoCK 2.1 in primary cultures of mouse hippocampal neurons. To express RocK 2.1, we utilized the AAV2/9 viral vector as shown in Fig 3.10C. Upon exiting the hippocampal neuron expressing RoCK 2.1 with a 10 ms light pulse at 525 nm at light intensities as low as 1.6 mW/mm², we observed a brief suppression of action potentials triggered by pulse current injections at AP threshold plus 50 pA (as depicted in Figure 3.10D). Notably, the duration of silencing intervals increased with rising light intensities.

Kleis et al., 2022 reported that the long-term use of the PACK system (first-generation tool) causes histological abnormalities such as cellular dispersion and astrogliosis in hippocampal tissue. To determine if the second-generation tool (RoCK) has similar long-term side effects, I expressed the RoCK tool into the hippocampus of mice and conducted immunohistochemistry. For histological analysis, RoCK-AAV was stereotaxically injected into the CA1 region of the mouse hippocampus (caudal diencephalon). 3-4 weeks post-injection, 50 µm brain coronal sections were immunostained for NeuN and GFAP to assess cellular dispersion and astrogliosis. (Fig 3.11A). After the injection, the RoCK 2.1 tool tagged with YFP fluorophore was expressed well in the CA1 region, as shown in Fig 3.11B.

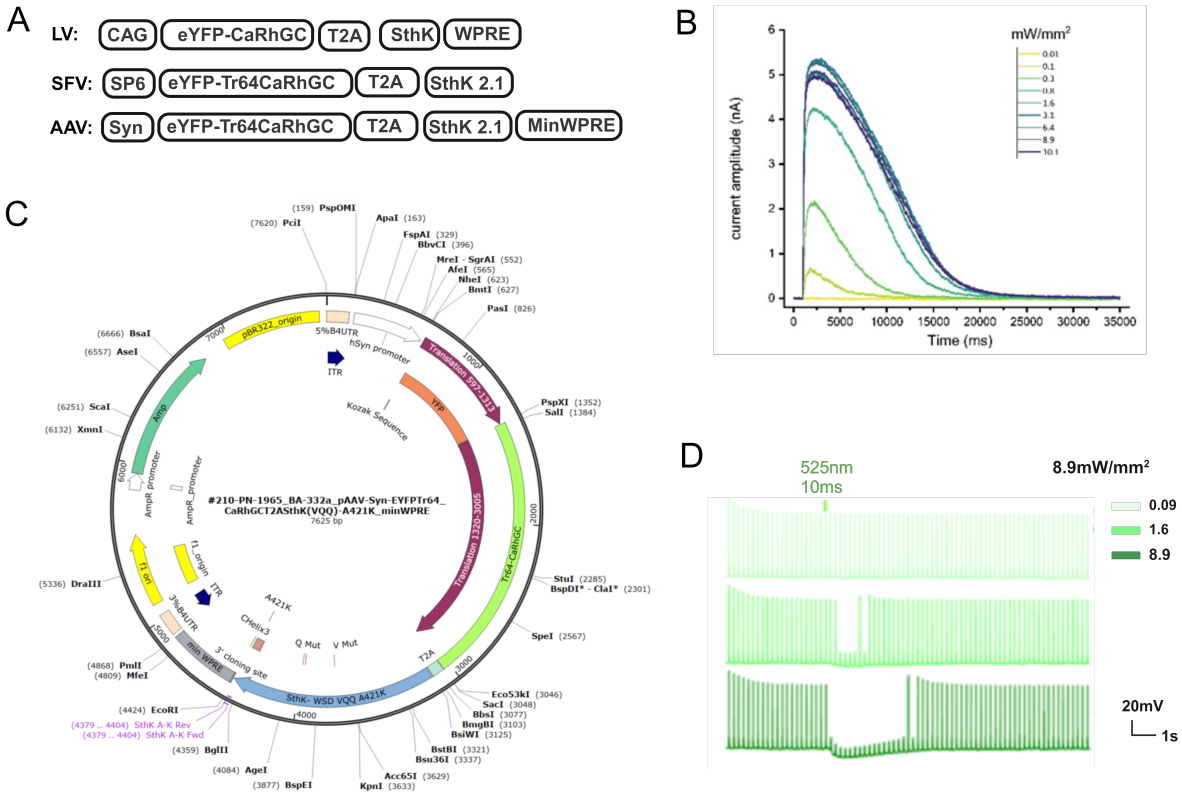

Figure 3.10: Optimization of RoCK 2.1. A. Configuration of the RoCK 2.1 constructs. The SthK WSD VQQ A421K mutant is named SthK 2.1 in the rest of the text. B, Sample traces of RoCK 2.1 at increasing light intensities, measured in ND 7/23 cells. C, AAV2/9 vector diagram of RoCK 2.1 used for mouse experiments. D, Example traces of pulse current injections (AP plus 50 pA) induced action potentials in the current clamp configuration showing the inhibition of AP firing in a neuron expressing RoCK 2.1. Courtesy: Anika Spreen, Yinth Andrea Bernal Sierra.

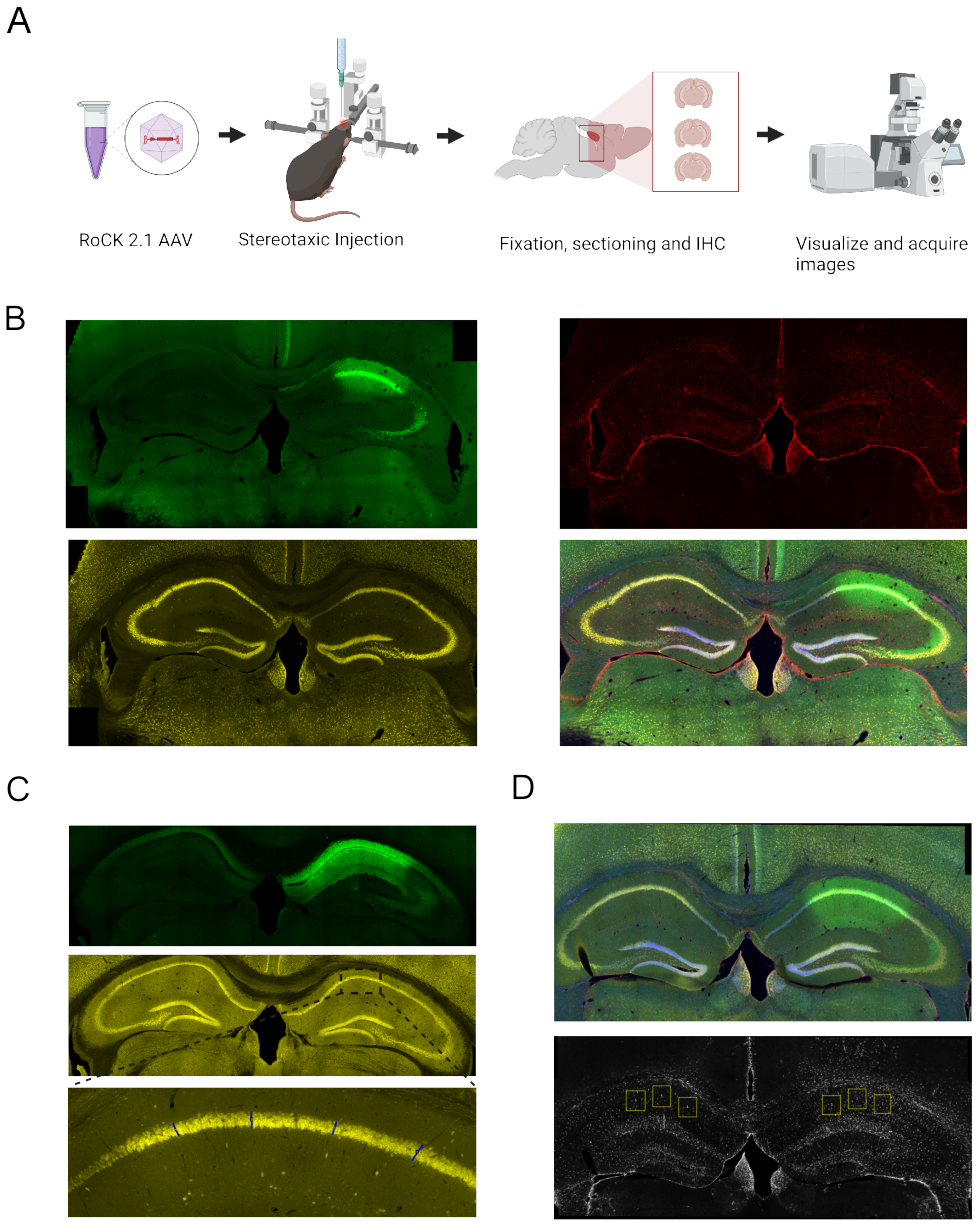

Figure 3.11: Hippocampus IHC after expressing RoCK 2.1 through AAV infection. A. Workflow for viral infection and Hippocampus imaging. B, Representative confocal immunofluorescent image (10X), RoCK-AAV (green), NeuN (yellow), and GFAP (red). The overlay image (20X) of the three stainings is demonstrated, where the cell nuclei are stained with DAPI (Blue). C, representative image (10X) of the hippocampal region stained with NeuN (yellow), RoCK-AAV expression is shown in green. The width of the CA1 pyramidal cell layer (in µm) was measured as an average length of 4 positions (blue lines), and compared between the right (RoCK 2.1 injected) and left (non-injected) hippocampus. D, The mean grey value of GFAP expression was measured in the CA1 (yellow box) in three sections per animal.

First, I conducted a measurement of cellular dispersion in the NeuN-labeled hippocampal slice. To do this, I calculated the difference between the width of the *stratum pyramidale* on both the injected and non-injected sides of hippocampus. I measured the width of the *stratum pyramidale* by taking an average of four perpendicular lines on the *stratum pyramidale* as illustrated in Figure 3.11C. Our results showed that the average width of the *stratum pyramidale* on the RoCK 2.1 injected side was 55.9 ± 1.85 μm, while it was 53 ± 0.71 μm on the non-injected side. It's worth noting that Kleis et al., 2022 observed a much larger difference in CA1 width in bPAC-expressing CA1 (19.45 ± 2.31 μm), and in PACK-expressing CA1 (10.98 ± 1.84 μm); the mCherry-expressing control group had a low value (1.86 ± 1.94 μm) (Fig 3.12B). To study the cellular changes induced by AAV, we injected a GFP-AAV as a control into the contralateral side and measured the differences also. The average width was 56.7 ± 4.3 μm (RoCK 2.1) and 57.7 ± 1.67 μm (n=3) (eGFP) (Fig 3.12B) respectively. Thus, the cellular dispersion of pyramidal neurons for the RoCK 2.1 tool is negligible.

To evaluate chronic astrogliosis, I compared the intensity of GFAP in the CA1 region, specifically in *stratum oriens*, *stratum pyramidale*, and *stratum radiatum*. I measured the mean grey value of three squares (ROI) and compared the results between the injected and non-injected sides of GFAP-stained brain slices (Fig 3.11D). The RoCK 2.1 tool showed a ratio of 1.33 ± 0.08 (n=3) between the injected and non-injected hippocampus. This value is similar to mCherry expressing in the CA1 region of the control group of Kleis et al., 2022, with a ratio of 1.26 (n=4). The intensity ratio of GFAP was significantly higher in bPAC mice, with a value of 3.11 (n=6) and in PACK-expressing mice, with a value of 2.4 (n=5) (Kleis et al., 2022) (Fig 3.12C). In addition, I compared the RoCK-AAV with GFP-AAV injected into the contralateral side (Fig 3.12A). The GFAP ratio between RoCK 2.1 and GFP is 1.8 ± 0.3 (n=3) (Fig 3.12C). These results suggest that incorporating the RoCK 2.1 tool leads to only small histological changes in the hippocampus compared with PACK and bPAC.

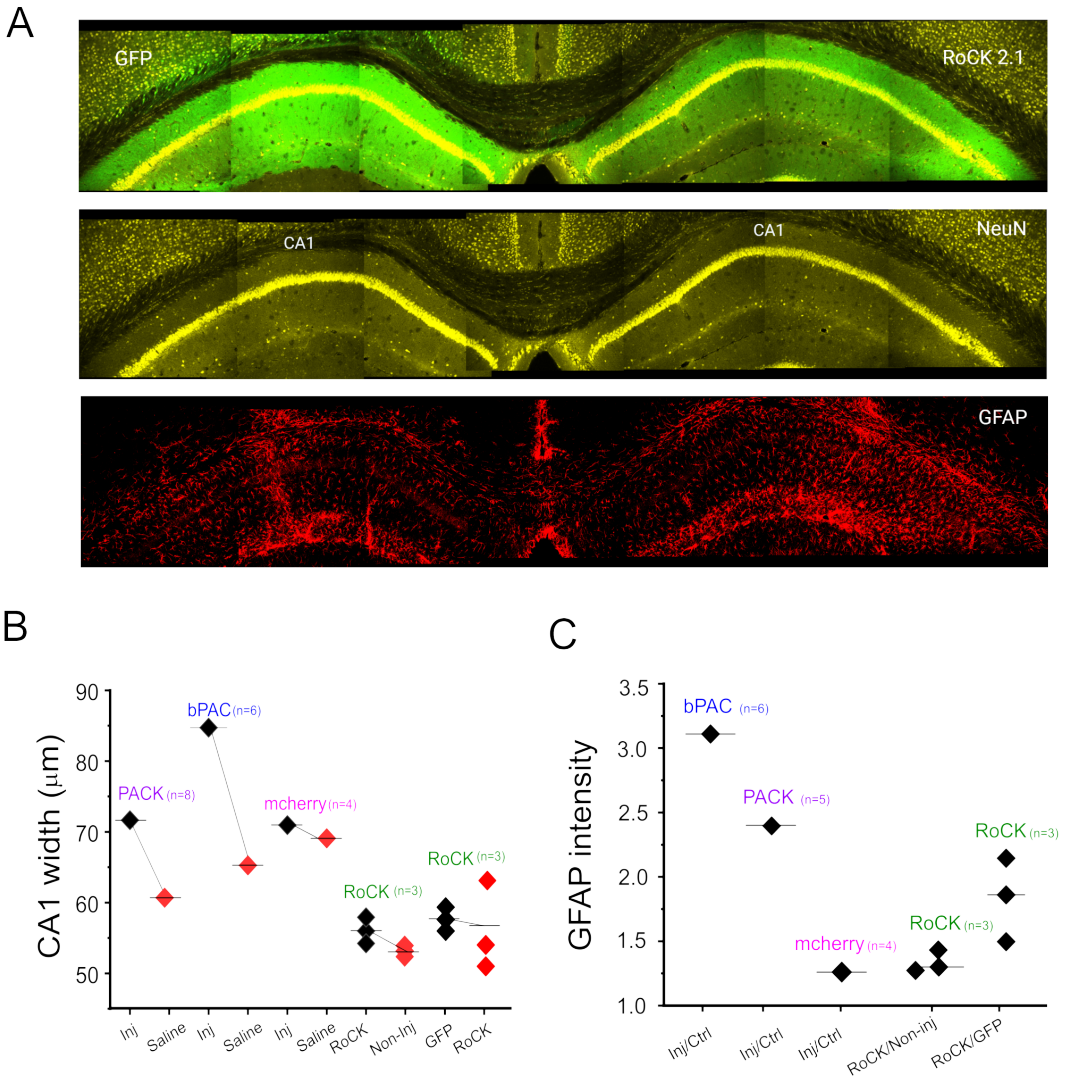

Figure 3.12: Comparison of RoCK 2.1 AAV and GFP AAV infection. A, Representative confocal immunofluorescent image (20X), RoCK-AAV and GFP-AAV (green), NeuN (yellow), and GFAP (red) after bilateral hippocampal injection, Right (RoCK-AAV) and left (GFP-AAV). B, The mean width of the CA1 pyramidal cell layer in RoCK AAV with non-infected and GFP-AAV (n=3), PACK, bPAC and mCherry (data for PACK, bPAC, and mCherry obtained from (Kleis et al., 2022)). C, The GFAP intensity of RoCK 2.1 injected CA1 is compared with non-infected, GFP, PACK, bPAC, and mCherry (data for PACK, bPAC, and mCherry obtained from (Kleis et al., 2022)).

4 Discussion

4.1 Applications of Optogenetic Tools

Optogenetics is an innovative technique in neuroscience that combines genetic and optical methods to control specific events within living tissue cells with high spatial and temporal precision. Light is being used to control excitable cells that have been genetically modified to express light-sensitive ion channels or pumps (Deisseroth, 2011). In the field of neuroscience, optogenetics allows researchers to modulate neural activity in a highly specific and controlled manner.

This technique has been instrumental in advancing our understanding of the nervous system and holds promise for therapeutic applications. The development of optogenetics has been a transformative journey spanning several decades, beginning with the discovery of light-sensitive proteins in microorganisms during the 1970s and 1980s. A breakthrough occurred in the early 2000s with the identification of Channelrhodopsins ChR1 and ChR2 in the green alga *Chlamydomonas reinhardtii*. The modern era of optogenetics began in 2005 when Karl Deisseroth and his team at Stanford University successfully introduced the gene encoding ChR2 into neurons (Boyden et al., 2005). Research in this field has been advancing swiftly, encompassing basic and industrial applications. The number of publications on the subject has increased from fewer than 100 to over 1,300 per year between 2010 and 2020. The number of articles in this scientific discipline has rapidly grown since 2010, with an annual growth rate of 52.82 % - indicating its significant development and relevance (Zhou et al., 2023).

4.1.1 Optogenetics in Basic Research

4.1.1.1 Dissecting Neural Circuits and Behavior

One of the key applications of optogenetics in fundamental research involves the analysis of neural circuits. Conventional brain study methods often lack the precision to target specific neurons or regulate their activity in real-time. Optogenetics addresses these limitations by allowing researchers to use light to activate or inhibit distinct groups of neurons. This precise control allows for better mapping of neural circuits and a deeper understanding of their roles in brain functions. The optogenetic technique significantly contributed to dissecting the neural circuits underlying complex behaviors and physiological processes (Swanson et al., 2022). For instance, researchers have been able to elucidate the roles of specific neuronal populations in processes such as sensory perception, motor control, and emotional regulation. Scientists can observe the changes in behavior and neural network dynamics, providing insights into the functional architecture of the brain. Studies have shown that stimulating specific neurons in the brain can trigger aggressive behavior, while inhibiting these neurons can reduce aggression (Tye & Deisseroth, 2012; Tye et al., 2011).

Optogenetics has advanced the exploration of synaptic plasticity, the cellular process fundamental to learning and memory (Sayegh et al., 2024). Researchers were able to accurately manipulate synaptic inputs and observe the subsequent alterations in synaptic effectiveness. This approach provides valuable insights into the molecular and cellular foundations of memory encoding and recall (Xie et al., 2013). This method also helps study the impact of genetic mutations, drugs, or environmental factors on synaptic plasticity and cognition, offering insights into neuropsychiatric disorders like Alzheimer's disease and schizophrenia.

Beyond basic research, optogenetics holds great promise for therapeutic applications, particularly in the treatment of neurological and psychiatric disorders. The ability to target specific neuronal populations with high precision makes optogenetics an attractive strategy for

modulating dysfunctional neural circuits associated with various diseases.

4.1.1.2 Neurological Disorders

In therapeutic applications, optogenetics offers a more refined and minimally invasive approach by selectively modulating specific neuronal pathways involved in the disease. Animal studies have shown that optogenetic stimulation of dopaminergic neurons in the midbrain can reduce motor deficits, thereby providing a potential pathway for developing more effective Deep Brain Stimulation therapies (Dagher et al., 2022; Gradinaru et al., 2009).

Optogenetics holds promise for treating Parkinson's disease by allowing control over neural circuits affected by the disorder. Traditional deep brain stimulation (DBS) can alleviate symptoms but lacks specificity. Optogenetics offers a refined approach by targeting specific neurons and circuits involved in motor control, potentially improving efficacy and reducing side effects (Fougère et al., 2021; Valverde et al., 2020).

In epilepsy, optogenetics can be used to modulate neural activity to prevent or stop seizures. By targeting and controlling the hyperactive neurons responsible for seizure activity, optogenetics provides a precise and potentially more effective treatment compared to current methods. This approach could lead to better management of epilepsy with fewer side effects (Kleis et al., 2022; Krook-Magnuson et al., 2013).

4.1.1.3 Psychiatric Disorders

Optogenetics also shows potential in treating psychiatric disorders such as depression, anxiety, and addiction. By modulating specific neural circuits involved in mood regulation and reward processing, researchers aim to restore normal function in these circuits. For example, optogenetic activation of the medial prefrontal cortex has been shown to alleviate depressive-like behaviors in animal models, suggesting a potential therapeutic strategy for treatment-resistant depression (Lin et al., 2022; Vialou et al., 2014).

4.1.1.4 Sensory Restoration

Another exciting application of optogenetics is in sensory restoration, particularly vision. Researchers are developing optogenetic approaches to restore vision in individuals with retinal degenerative diseases. Introducing light-sensitive proteins into the remaining retinal cells can make these cells responsive to light, partially restoring visual function. This approach is currently being tested in clinical trials, potentially providing significant improvements in vision for patients with conditions like retinitis pigmentosa (Bi et al., 2006; Klapoetke et al., 2014; Scholl et al., 2016). While current approaches target ganglion cells, new tools target bipolar cells, potentially restoring higher-quality vision. Bipolar cell-targeted optogenetics could significantly improve vision in patients with advanced retinal degeneration (Kralik et al., 2022).

4.1.1.5 Neuropathic pain

Optogenetics is used to study pain behavior and the underlying neural circuit and hold the potential for relatively non-invasive and direct therapeutic strategies to treat peripheral pain (Iyer et al., 2014; Zachariou & Carr, 2014).

4.1.1.6 Cancer

In cancer research, optogenetics can be used to precisely control the activity of immune cells and cancer cells. This method could enhance the accuracy of cancer treatments by targeting tumor cells more effectively while minimizing harm to healthy tissue. It can activate the immune response, stimulate oncolytic activity, and modulate cell signaling in tumor cells non-invasively (Zhou et al., 2018). Additionally, it offers a dose-controlled, tissue-specific action without the side effects of conventional therapies.

4.1.1.7 Spinal Cord Injury

Optogenetics represent a potential breakthrough in treating spinal cord injuries and rehabilitation and therapy. Modulating neuron activity with high precision, optogenetics can facilitate neural regeneration and functional recovery. This approach involves the use of light-sensitive proteins to selectively stimulate neurons and modulate neural circuits, which can improve motor function and sensory perception. Studies have demonstrated that this technique can effectively target specific neurons and pathways (Ahmad et al., 2015; Deng et al., 2021).

4.1.2 Role of Optogenetics in Enzyme Control

Nowadays, optogenetics is extensively employed in both clinical and industrial settings to control enzymatic activity and regulate cellular metabolism. By utilizing light-sensitive proteins, optogenetics enables precise spatial and temporal regulation of enzyme functions in biochemical applications. This technique allows for the control of specific enzymes such as Phosphodiesterases (PDEs), protein kinase A (PKA), and Guanylate Cyclases (GCs), which play crucial roles in various cellular processes.

By using light-sensitive domains, these enzymes can be modulated:

1. Phosphodiesterases (PDEs): Regulate the levels of cyclic nucleotides (cAMP and cGMP) in cells. Optogenetic control of PDEs enables detailed studies of cyclic nucleotide signaling pathways and their roles in cellular functions and disease mechanisms (Stabel et al., 2019; Tian et al., 2020).

2. Protein Kinase A (PKA): PKA is involved in cellular processes like metabolism, gene expression, and memory. Optogenetic tools can investigate the dynamic roles of PKA in these processes (Yi et al., 2014), providing insights into its dysregulation in diseases like cancer and diabetes (Leopold et al., 2018).

3. Guanylate Cyclases (GCs): Catalyze the conversion of GTP to cGMP, a signaling

molecule involved in vision, vasodilation, and cellular proliferation. Optogenetic modulation of GCs provides a method to study cGMP signaling pathways in real-time, with applications in understanding the cardiovascular function and developing treatments for related disorders (Gao et al., 2015).

4.1.3 Optogenetics in Industry

Optogenetics has become widely utilized in the industrial sector to enhance the efficiency and precision of biochemical reactions. Its increasing popularity spans various sectors, including pharmaceuticals, biofuels, and other valuable compounds, due to its capacity to precisely control key enzymes in metabolic pathways, thereby improving product quality (Kim et al., 2012; Reshetnikov et al., 2022).

In bioprocessing and biotechnology, optogenetics enables the precise regulation of metabolic pathways in microorganisms, leading to improved chemical production. Managing bacterial gene expression through optogenetics is becoming a well-established method, with potential future applications focusing on direct protein-based control of biological processes (Brechun et al., 2017; Ohlendorf & Möglich, 2022; Shimizu-Sato et al., 2002). Light-sensitive domains can be combined with DNA-binding domains like dCas9, zinc finger nucleases, TALENs, transcriptional activators or repressors (e.g., VP16 or KRAB), and protein-binding domains such as nanobodies (Gil et al., 2020; Mansouri et al., 2019). Optogenetics also benefits the pharmaceutical industry by facilitating the development of more precise disease models in drug discovery and cell-based therapies (Tan et al., 2022; Ye et al., 2011). In synthetic biology, light-controlled gene expression and metabolic activities enable the creation of programmable cells and organisms capable of performing complex tasks such as biosensing and environmental remediation. Optogenetics is a versatile tool with precise control over biological processes, opening up new possibilities for innovation and efficiency in industry. These diverse applications underscore the transformative potential of optogenetics across various scientific fields.

4.2 Inhibitory Tools in Optogenetics

In neuroscience research, inhibitory tools in optogenetics are crucial, just as excitatory tools are. Inhibition is achieved by employing light-sensitive proteins to silence specific neurons selectively. Inhibitory optogenetics also holds promise for therapeutic applications, such as targeting and suppressing overactive neurons to treat neurological disorders. By enabling in-depth study and manipulation of neural networks, inhibitory tools significantly advance our understanding of both brain function and dysfunction.

4.2.1 Types of Inhibitory Tools

Halorhodopsin (NpHR), Archaerhodopsin (ArchT), and Anion Channelrhodopsins (ACRs) are optogenetic tools commonly used to inhibit neuronal activity. These tools enable reversible and precise silencing of neurons with high temporal resolution. However, all these have some drawbacks that restrict their application.

Potassium-based inhibitory tools are divided into natural potassium selective Channelrhodopsins (KCRs) and engineered systems. KCRs are naturally occurring proteins that can be genetically engineered or utilized directly in optogenetic experiments. When exposed to specific wavelengths of light, they permit potassium ions to pass through, resulting in cell membrane hyperpolarization and the inhibition of neuronal firing. Recently discovered members of this protein family, HcKCR1 and HcKCR2, can attenuate neuronal activity upon light activation. Their application in optogenetic research allows for the selective suppression of neurons within a targeted population. WiChR is a variant of Channelrhodopsin from *W.lunata*, which demonstrates a high degree of precision and efficiency in conducting potassium ions. Its recent development has yielded enhanced attributes such as heightened light sensitivity and improved kinetics, rendering it an invaluable instrument for in-depth examination of neural circuits at an elevated temporal resolution (Vierock et al., 2022).

Other engineered systems, tools such as BLINK 1/2 and PACK (Alberio et al., 2018; Bernal Sierra et al., 2018; Cosentino et al., 2015) utilize LOV2 domains as light sensors. While BLINK and PACK offer high operational cellular light sensitivity, they come with certain limitations. For instance, BLINK 1/2 exhibits very slow on-and-off kinetics, and PACK displays some dark activity. Furthermore, it is challenging to adjust absorption in any photoreceptor containing a flavin chromophore. This is where the RoCK 2.1 system excels, offering a novel approach that overcomes these limitations. We have developed RoCK 2.1 (as shown in Fig 4.1), a novel two-component optogenetic silencing tool. This tool combines the modified SthK channel and Rhodopsin Guanylyl Cyclase.

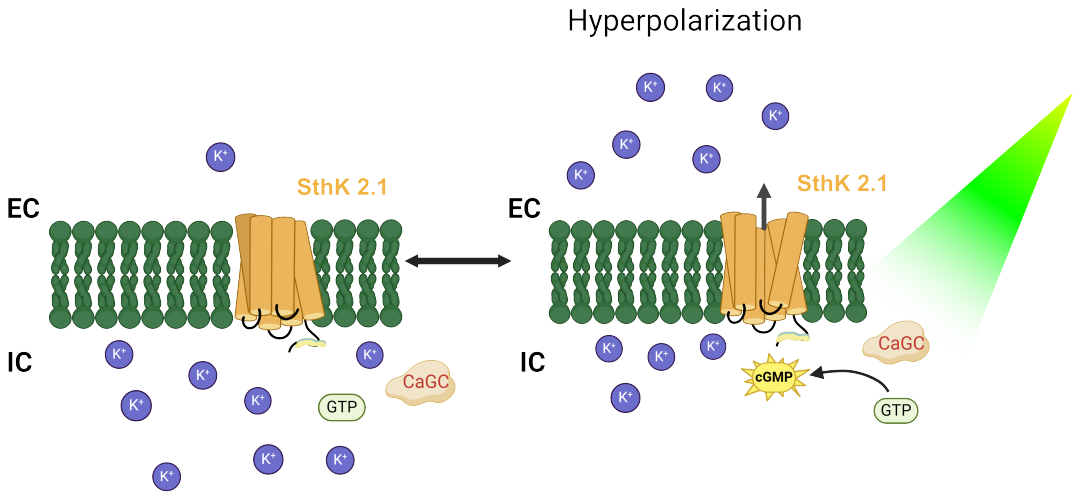

Figure 4.1: Illustration of RoCK 2.1.

One of the key features of RoCK 2.1 is its adaptability to various experimental setups and systems. Its primary benefit lies in its ability to significantly amplify signals, thereby minimizing the photon budget required. The Rhodopsin Guanylyl Cyclase used can be color-tuned from green to red. The sensitivity of the tool can also be adjusted by combining it with varying mutant channels (Fig 3.10A), providing a range of sub-micromolar to micromolar cGMP sensitivity, making it applicable to cells with high cGMP turnover.

Our main goal was to use cGMP as a second messenger to minimize interference with metabolic processes. RhGCs meet this requirement by producing cGMP when exposed

to light, in contrast to bPAC, which produces cAMP in the PACK system. The use of cGMP as a ligand results in minimal dark activity due to the low endogenous cGMP in cells and low dark activity of the RhGC enzymes.

In our initial quest for a cGMP-gated potassium-selective channel, we identified several potential candidates, including the ApCNGK channel from sea urchin sperm (Bönigk et al., 2009). The ApCNGK channel, known for its high sensitivity to cGMP, was initially considered due to its promising characteristics. However, trafficking of the channel in mammalian cells was malfunctioning at 37 °C, necessitating low-temperature conditions incompatible with in vivo applications. Additionally, the large pseudo-tetrameric structure of the CNGK channel posed significant challenges for efficient packaging into adeno-associated virus (AAV) vectors, limiting its practical application. Given these limitations, we decided to use the wild-type (Wt) SthK channel and modify it to better suit our needs. The SthK channel has been successfully employed in the PACK system for heterologous expression, and its structural details and biophysical properties are well documented. Furthermore, the SthK channel shares structural homology with other CNG channels, making it a suitable candidate for our modifications.

We did four rounds of mutations to the SthK channel in the course of this study. Initial ligand binding in cyclic nucleotide-binding domains (CNBDs) involves the phosphate-binding cassette (PBC) motif located in the β-roll of the CNBD. In the SthK channel, these are interactions of the ligand with Gly-367, Glu-368, Thr-378, and Arg-377 (Kesters et al., 2015; Pan et al., 2023).

When a ligand binds to the PBC in CNG or HCN channels, it causes the C-helix to move towards the β-roll of the CNBD, stabilizing the open state of the channel (Kesters et al., 2015; Pan et al., 2023). This triggers conformational changes that lead to the opening of the channel pore (Kesters et al., 2015; Morgan et al., 2019; Schmidpeter et al., 2018). The significance of the C-helix in cyclic nucleotide selectivity and channel activation mechanisms is highlighted by research on channels like CNGA1 and HCN2 (Ng et al., 2019;

Varnum et al., 1995).

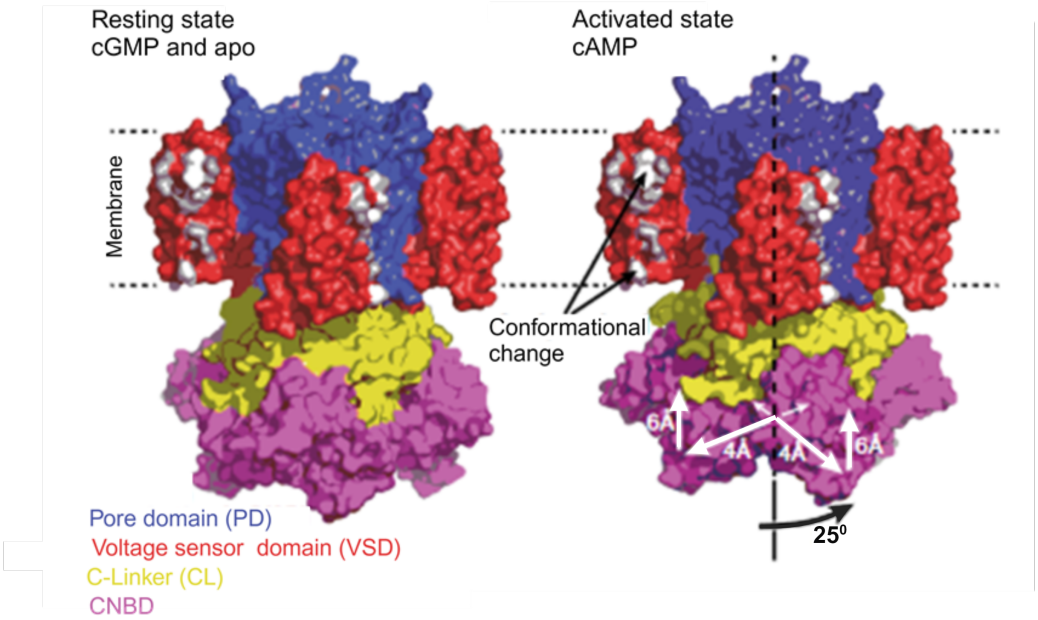

Figure 4.2: Channel gating mechanism. The conformational changes in SthK upon activation (Adapted from Marchesi et al., 2018

Our initial approach involved replacing the C-helix of the SthK channel to alter the ligand selectivity and responsiveness. The mutant displayed an increase in cGMP responsiveness, albeit far from being a good candidate channel.

The introduction of three additional point mutations resulted in a marked shift in cyclic nucleotide selectivity. There was a significant increase in the open probability specifically for cGMP, while there was a pronounced decrease in the channel's open probability for cAMP. This change underscored the heightened sensitivity of the channel to cGMP compared to cAMP. These findings emphasize the efficacy of targeted mutations in altering ligand selectivity and channel behavior and demonstrate the potential to improve channel function through precise genetic modifications. These mutations were inspired from research on eukaryotic CNG channels, highlighting their relevance to the prokaryotic channel context.

The C-linker region plays a significant role in channel opening, as initially proposed by Gordon and Zagotta (Gordon & Zagotta, 1995a; Gordon & Zagotta, 1995b). We explored the pivotal role of the C-linker region in channel opening, a crucial aspect of channel function. Structural changes within the CNBD that interact with the C-linker are well-documented in the hHCN1 channel (Kondapuram et al., 2020; Lolicato et al., 2011; Xu et al., 2010; Zagotta et al., 2003) and in the TAX-4 channel (Zheng et al., 2020). In the rod CNG channel, mutational studies highlighted that amino acids in the C-linker region could improve the channel's responsiveness (Paoletti et al., 1999; Zong et al., 1998). Recent research on the HCN channel suggests that ligand binding to CNBD may stabilize the channel's open state by causing a rotational motion of the C-linker, which widens the pore (Gross et al., 2018). In our experiments with the SthK 1.0 channel, introducing the S6 and C-linker mutations (A208V, R284Q, and E290Q) significantly increased both open probability and sensitivity. These results align with findings from previous studies (Morgan et al., 2019; Paoletti et al., 1999), highlighting the enhanced sensitivities of the modified SthK 2.0 channel to both cGMP and cAMP. Our findings also underscore the role of the C-linker region in regulating channel function and ligand responsiveness.

Our study focused on enhancing the functionality of the SthK channel for optimal performance for our silencing tool application. A key objective was to increase cGMP specificity while minimizing cAMP sensitivity, thereby improving channel efficacy. The introduction of a mutation replacing Alanine 421 with Lysine, inspired by findings from the TAX-4 channel (Li et al., 2017), proved effective. In our channel, the mutation enhances specificity for cGMP and improves the channel's open probability. The increase in open probability was particularly pronounced in SthK 1.1, where we observed a 1.8 fold increase. In SthK 2.1, the increase in open probability was only by 1.14 fold. In addition, SthK 1.1 exhibited the highest fractional current I(cGMP)/I(cAMP) among the variants studied.

The different impact of the A421K mutation observed between SthK 1.1 and SthK 2.1 highlight the role of C-linker mutations. In SthK 2.1, these mutations promote an open

channel state, potentially moderating the influence of additional interactions that also stabilize that state. In contrast, the absence of C-linker mutations in SthK 1.1 underscores the importance of interactions stabilizing the bound cGMP for effective channel activation and selective responsiveness of the channel. These findings underscore the strategic use of targeted mutations to tailor channel properties, enhancing their suitability for specific applications.

Future research could further explore such mutations among different members of the CNG channel family. How do their structural differences influence channel dynamics and expand their potential applications in biological and technological contexts requiring precise ligand discrimination and channel functionality?

4.3 Candidate channels

Our mutational journey resulted in three candidate channels (SthK 1.1, 2.0, and 2.1) with slightly different properties that may be selected for the RoCK tool in different circumstances. SthK 1.1 is the channel that discriminates best between the desired ligand cGMP and the undesired ligand cAMP. However, this channel has a slightly lower maximal open probability and also a slightly lower sensitivity towards cGMP. SthK 2.0 has the highest affinity for cGMP ($K_{1/2}$=220 nM) and a maximal open probability of 0.35 at physiological voltages. In combination with RhGC, SthK 2.0 performed best in terms of transported K+ ions per light dose due to its high ligand affinity (Anika Spreen, personal communication). This performance was accompanied with a slow closing rate after light off, which may be viewed as an advantage (more inhibition) or disadvantage (less control). Finally, SthK 2.1 has the highest open probability of the candidates and, compared to SthK 2.0, an improved ligand selectivity. Combined with RhGC, it displays, together with SthK 2.0, the highest light-induced currents but faster off kinetics, compared with SthK 2.0 (Anika Spreen, personal communication).

We selected SthK 2.1 to study, how the tool performs in our initial applications.

4.4 Application of RoCK 2.1

With regards to long-term application, PACK is so far the only silencing tool that has been applied to successfully inhibit action potentials in healthy and chronically afflicted epileptic behaving mice. The long-term use of the PACK system showed increased light-independent neuronal activity, causing unwanted side effects such as spontaneous generalized seizures. Cytological changes in the hippocampus like the widening of the stratum pyramidale and astrogliosis were observed. The authors of the study concluded that cAMP signaling was responsible for these cytological changes, most likely due to the significant dark activity of bPAC (Kleis et al., 2022). Pyramidal neurons of CA1 in the hippocampus show increased susceptibility to insults such as ischemia, inflammation, hypoglycemia, and excitotoxicity compared to CA3 and the dentate gyrus (Bramlett et al., 1999). Therefore, we conducted immunohistochemistry to evaluate potential cytological changes resulting from RoCK-AAV injection or RoCK 2.1 expression and activity in the mouse hippocampus. We introduced RoCK 2.1 into the mouse hippocampus, both with and without the control (GFP) injected in the contralateral side. Our IHC results show no significant changes in the widening of the neuronal cell layer, as Kleis et al., 2022 reported using the bPAC or the PACK system.

In addition, we observed only mild astrogliosis in both the control groups, with and without GFP. Previous studies have demonstrated that intracerebral injection of adenovirus often induces severe neuroinflammation, including reactive astrogliosis (Chun et al., 2020; Woo et al., 2017). It's important to note that while we detected the expression of the RoCK 2.1 in the hippocampus (Fig 3.10 B, 3.11 A), we have not yet investigated the function of Rock 2.1 in these hippocampal neurons. Our in vivo experiments revealed that cytological changes induced by RoCK 2.1 expression are small compared to the previous PACK system. Further studies are required to investigate the performance of the RoCK 2.1 tool in hippocampal neurons.

RoCK 2.1 offers advantages over previously reported cAMP-dependent systems like PACK. First, RoCK 2.1 demonstrates a higher specificity for the second messenger cGMP over cAMP. In the majority of tissues, with few exceptions, the cGMP concentration is very low compared to cAMP (Hartwig et al., 2014). Thus, we can minimize the light-independent activity of the optogenetic tool. Previous studies reported this dark activity of the PACK system in *C. elegans* (Henß et al., 2022) and mice (Kleis et al., 2022). Second, CaRhGC exhibits a very small dark activity and, therefore, minimizes the risk of side effects associated with constant and increased activation of cGMP signaling pathways. However, we expect there might be some cGMP-induced activity for RoCK 2.1 in tissues with high endogenous cGMP, such as vascular endothelial tissues and specific neuronal cells. To assess this, further studies are needed. Finally, testing RoCK 2.1 in various heterologous systems, RoCK 2.1 performed better than the PACK system in terms of higher photo-induced current amplitude with low operational light intensity (Anika Spreen, personal communication). The expression of RoCK 2.1 did not affect the biophysical properties of neurons, such as resting membrane potential and membrane time constant.

In summary, RoCK 2.1 stands as a valuable addition to the repertoire of potassium-based silencing tools. Its reliance on cGMP and absence of dark activity position it as a promising alternative in model systems where elevated cAMP levels could induce unwanted side effects. Moreover, we emphasize the versatility of its individual components. While CaRhGC can serve as a cGMP actuator, modified SthK can be used as a tool for investigating cGMP signaling pathways. Available cGMP sensors face limitations in dynamic range, temporal resolution, and specificity due to the low concentrations of cellular cGMP (Argyrousi et al., 2020; Kleppisch & Feil, 2009). In contrast, SthK 2.1 provides the capability to explore cGMP-mediated processes either by monitoring direct cGMP production with millisecond precision, or by characterization of cGMP effectors such as PDEs and GCs.

5 Abstract

In Optogenetics, light is used to regulate the cellular activity. Most optogenetic tools are excitatory, and few are for inhibition. Recently, researchers developed a Potassium ion (K^+) based artificial two-component optogenetic tool for silencing of excitable cells. However, this tool has a few drawbacks, like cAMP-induced secondary side effects in the host cell and slow channel kinetics. A channel using cGMP as a ligand could maybe abate these problems.

Here in this project, I engineered a cGMP-gated K^+ channel for the 2nd generation of the two-component optogenetic silencing tool. For this purpose, we selected a cAMP-gated potassium channel from the bacteria *Spirochaeta thermophila* (SthK) as the candidate channel. We replaced a portion of the Cyclic Nucleotide-Binding domain (CNBD) of the SthK channel with that of another cGMP-gated channel. In addition, by inducing additional point mutations at the C-helix region and other cytoplasmic domain regions, we could switch the ligand selectivity and enhance the open probability of the ion channel. Finally, our engineered channel is highly cGMP sensitive (660 nM) with a small residual agonistic activity of cAMP. Our final mutant channel (SthK 2.1) has been combined with light-activated Guanylyl Cyclase to form RoCK 2.1, an efficient two-component optogenetic silencing tool for silencing of excitable cells. In this study, we introduced the AAV-incorporated silencing tool (RoCK 2.1) into the hippocampus of a mouse model and investigated its potential adverse effects through immunohistological methods.

6 List of Figures

7 List of Tables

8 References

Ahmad, A., Ashraf, S., & Komai, S. (2015). Optogenetics Applications for Treating Spinal Cord Injury. *Asian Spine Journal*, *9*(2), 299–305. https://doi.org/10.4184/asj.2015.9.2.299

Alberio, L., Locarno, A., Saponaro, A., Romano, E., Bercier, V., Albadri, S., Simeoni, F., Moleri, S., Pelucchi, S., Porro, A., Marcello, E., Barsotti, N., Kukovetz, K., Boender, A. J., Contestabile, A., Luo, S., Moutal, A., Ji, Y., Romani, G., … Moroni, A. (2018). A light-gated potassium channel for sustained neuronal inhibition. *Nature Methods*, *15*(11), 969–976. https://doi.org/10.1038/s41592-018-0186-9

Alfonsa, H., Merricks, E. M., Codadu, N. K., Cunningham, M. O., Deisseroth, K., Racca, C., & Trevelyan, A. J. (2015). The contribution of raised intraneuronal chloride to epileptic network activity. *The Journal of Neuroscience: The Official Journal of the Society for Neuroscience*, *35*(20), 7715–7726. https://doi.org/10.1523/JNEUROSCI.4105-14.2015

Altenhofen, W., Ludwig, J., Eismann, E., Kraus, W., Bönigk, W., & Kaupp, U. B. (1991). Control of ligand specificity in cyclic nucleotide-gated channels from rod photoreceptors and olfactory epithelium. *Proceedings of the National Academy of Sciences*, *88*(21), 9868–9872. https://doi.org/10.1073/pnas.88.21.9868

Andersson, J., Kleinheinz, D., Ramach, U., Kiesenhofer, N., Ashenden, A., Valtiner, M., Holt, S., Koeper, I., Schmidpeter, P. A. M., & Knoll, W. (2023). Native Function of the Bacterial Ion Channel SthK in a Sparsely Tethered Lipid Bilayer Membrane Ar-

chitecture. *The Journal of Physical Chemistry B*, *127*(16), 3641–3650. https://doi.org/10.1021/acs.jpcb.2c07252

Argyrousi, E. K., Heckman, P. R. A., & Prickaerts, J. (2020). Role of cyclic nucleotides and their downstream signaling cascades in memory function: Being at the right time at the right spot. *Neuroscience and Biobehavioral Reviews*, *113*, 12–38. https://doi.org/10.1016/j.neubiorev.2020.02.004

Banghart, M., Borges, K., Isacoff, E., Trauner, D., & Kramer, R. H. (2004). Light-activated ion channels for remote control of neuronal firing. *Nature Neuroscience*, *7*(12), 1381–1386. https://doi.org/10.1038/nn1356

Barry, P. H. (1994). JPCalc, a software package for calculating liquid junction potential corrections in patch-clamp, intracellular, epithelial and bilayer measurements and for correcting junction potential measurements. *Journal of Neuroscience Methods*, *51*(1), 107–116. https://doi.org/10.1016/0165-0270(94)90031-0

Beck, S., Yu-Strzelczyk, J., Pauls, D., Constantin, O. M., Gee, C. E., Ehmann, N., Kittel, R. J., Nagel, G., & Gao, S. (2018). Synthetic Light-Activated Ion Channels for Optogenetic Activation and Inhibition. *Frontiers in Neuroscience*, *12*. https://doi.org/10.3389/fnins.2018.00643

Bernal Sierra, Y. A., Rost, B. R., Pofahl, M., Fernandes, A. M., Kopton, R. A., Moser, S., Holtkamp, D., Masala, N., Beed, P., Tukker, J. J., Oldani, S., Bönigk, W., Kohl, P., Baier, H., Schneider-Warme, F., Hegemann, P., Beck, H., Seifert, R., & Schmitz, D. (2018). Potassium channel-based optogenetic silencing. *Nature Communications*, *9*(1), 4611. https://doi.org/10.1038/s41467-018-07038-8

Berndt, A., Lee, S. Y., Ramakrishnan, C., & Deisseroth, K. (2014). Structure-guided transformation of channelrhodopsin into a light-activated chloride channel. *Science (New York, N.Y.)*, *344*(6182), 420–424. https://doi.org/10.1126/science.1252367

Bi, A., Cui, J., Ma, Y.-P., Olshevskaya, E., Pu, M., Dizhoor, A. M., & Pan, Z.-H. (2006). Ectopic Expression of a Microbial-Type Rhodopsin Restores Visual Responses in Mice with Photoreceptor Degeneration. *Neuron*, *50*(1), 23–33. https://doi.org/10.1016/j.neuron.2006.02.026

Bönigk, W., Loogen, A., Seifert, R., Kashikar, N., Klemm, C., Krause, E., Hagen, V., Kremmer, E., Strünker, T., & Kaupp, U. B. (2009). An atypical CNG channel activated by a single cGMP molecule controls sperm chemotaxis. *Science Signaling*, *2*(94), ra68. https://doi.org/10.1126/scisignal.2000516

Bramlett, H. M., Green, E. J., & Dietrich, W. D. (1999). Exacerbation of cortical and hippocampal CA1 damage due to posttraumatic hypoxia following moderate fluid-percussion brain injury in rats. https://doi.org/10.3171/jns.1999.91.4.0653

Brams, M., Kusch, J., Spurny, R., Benndorf, K., & Ulens, C. (2014). Family of prokaryote cyclic nucleotide-modulated ion channels. *Proceedings of the National Academy of Sciences*, *111*, 7855–7860. https://doi.org/10.1073/pnas.1401917111

Brechun, K. E., Arndt, K. M., & Woolley, G. A. (2017). Strategies for the photo-control of endogenous protein activity. *Current Opinion in Structural Biology*, *45*, 53–58. https://doi.org/10.1016/j.sbi.2016.11.014

Chow, B. Y., Han, X., Dobry, A. S., Qian, X., Chuong, A. S., Li, M., Henninger, M. A., Belfort, G. M., Lin, Y., Monahan, P. E., & Boyden, E. S. (2010). High-performance genetically targetable optical neural silencing by light-driven proton pumps. *Nature*, *463*(7277), 98–102. https://doi.org/10.1038/nature08652

Chun, H., Im, H., Kang, Y. J., Kim, Y., Shin, J. H., Won, W., Lim, J., Ju, Y., Park, Y. M., Kim, S., Lee, S. E., Lee, J., Woo, J., Hwang, Y., Cho, H., Jo, S., Park, J.-H., Kim, D., Kim, D. Y., … Lee, C. J. (2020). Severe reactive astrocytes precipitate pathological hallmarks of Alzheimer's disease via H2O2− production. *Nature Neuroscience*, *23*(12), 1555–1566. https://doi.org/10.1038/s41593-020-00735-y

Copits, B. A., Gowrishankar, R., O'Neill, P. R., Li, J.-N., Girven, K. S., Yoo, J. J., Meshik, X., Parker, K. E., Spangler, S. M., Elerding, A. J., Brown, B. J., Shirley, S. E., Ma, K. K. L., Vasquez, A. M., Stander, M. C., Kalyanaraman, V., Vogt, S. K., Samineni, V. K., Patriarchi, T., … Bruchas, M. R. (2021). A photoswitchable GPCR-based opsin for presynaptic inhibition. *Neuron*, *109*(11), 1791–1809.e11. https://doi.org/10.1016/j.neuron.2021.04.026

Cosentino, C., Alberio, L., Gazzarrini, S., Aquila, M., Romano, E., Cermenati, S., Zuccolini, P., Petersen, J., Beltrame, M., Van Etten, J. L., Christie, J. M., Thiel, G., & Moroni, A. (2015). Engineering of a light-gated potassium channel. *Science*, *348*(6235), 707–710. https://doi.org/10.1126/science.aaa2787

Dagher, M., Perrotta, K. A., Erwin, S. A., Hachisuka, A., Iyer, R., Masmanidis, S. C., Yang, H., & Andrews, A. M. (2022). Optogenetic Stimulation of Midbrain Dopamine Neurons Produces Striatal Serotonin Release. *ACS chemical neuroscience*, *13*(7), 946–958. https://doi.org/10.1021/acschemneuro.1c00715

Das, R., Chowdhury, S., Mazhab-Jafari, M. T., SilDas, S., Selvaratnam, R., & Melacini, G. (2009). Dynamically Driven Ligand Selectivity in Cyclic Nucleotide Binding Domains *. *Journal of Biological Chemistry*, *284*(35), 23682–23696. https://doi.org/10.1074/jbc.M109.011700

Deisseroth, K. (2011). Optogenetics. *Nature methods*, *8*(1), 26–29. https://doi.org/10.1038/nmeth.f.324

Deng, W.-W., Wu, G.-Y., Min, L.-X., Feng, Z., Chen, H., Tan, M.-L., Sui, J.-F., Liu, H.-L., & Hou, J.-M. (2021). Optogenetic Neuronal Stimulation Promotes Functional Recovery After Spinal Cord Injury. *Frontiers in Neuroscience*, *15*, 640255. https://doi.org/10.3389/fnins.2021.640255

Dutar, P., Petrozzino, J. J., Vu, H. M., Schmidt, M. F., & Perkel, D. J. (2000). Slow Synaptic Inhibition Mediated by Metabotropic Glutamate Receptor Activation of GIRK Chan-

nels. *Journal of Neurophysiology*, *84*(5), 2284–2290. https://doi.org/10.1152/jn.2000.84.5.2284

Evans, E. G. B., Morgan, J., DiMaio, F., Zagotta, W. N., & Stoll, S. (2020). Allosteric conformational change of a cyclic nucleotide-gated ion channel revealed by DEER spectroscopy. *Proceedings of the National Academy of Sciences*, *117*, 10839–10847. https://doi.org/10.1073/pnas.1916375117

Fischer, P., Mukherjee, S., Schiewer, E., Broser, M., Bartl, F., & Hegemann, P. (2021). The inner mechanics of rhodopsin guanylyl cyclase during cGMP-formation revealed by real-time FTIR spectroscopy (B. Chanda, K. J. Swartz, & H. Kandori, Eds.). *eLife*, *10*, e71384. https://doi.org/10.7554/eLife.71384

Fougère, M., van der Zouwen, C. I., Boutin, J., Neszvecsko, K., Sarret, P., & Ryczko, D. (2021). Optogenetic stimulation of glutamatergic neurons in the cuneiform nucleus controls locomotion in a mouse model of Parkinson's disease. *Proceedings of the National Academy of Sciences*, *118*(43), e2110934118. https://doi.org/10.1073/pnas.2110934118

Gao, S., Nagpal, J., Schneider, M. W., Kozjak-Pavlovic, V., Nagel, G., & Gottschalk, A. (2015). Optogenetic manipulation of cGMP in cells and animals by the tightly light-regulated guanylyl-cyclase opsin CyclOp. *Nature Communications*, *6*(1), 8046. https://doi.org/10.1038/ncomms9046

Gil, A. A., Carrasco-López, C., Zhu, L., Zhao, E. M., Ravindran, P. T., Wilson, M. Z., Goglia, A. G., Avalos, J. L., & Toettcher, J. E. (2020). Optogenetic control of protein binding using light-switchable nanobodies. *Nature Communications*, *11*(1), 4044. https://doi.org/10.1038/s41467-020-17836-8

Gordon, S. E., & Zagotta, W. N. (1995a). Subunit interactions in coordination of Ni2+ in cyclic nucleotide-gated channels. *Proceedings of the National Academy of Sciences of the United States of America*, *92*(22), 10222–10226

Gordon, S. E., & Zagotta, W. N. (1995b). Localization of regions affecting an allosteric transition in cyclic nucleotide-activated channels. *Neuron*, *14*(4), 857–864. https://doi.org/10.1016/0896-6273(95)90229-5

Goulding, E. H., Tibbs, G. R., & Siegelbaum, S. A. (1994). Molecular mechanism of cyclic-nucleotide-gated channel activation. *Nature*, *372*(6504), 369–374. https://doi.org/10.1038/372369a0

Govorunova, E. G., Gou, Y., Sineshchekov, O. A., Li, H., Wang, Y., Brown, L. S., Xue, M., & Spudich, J. L. (2021). Kalium rhodopsins: Natural light-gated potassium channels, 2021.09.17.460684. https://doi.org/10.1101/2021.09.17.460684

Govorunova, E. G., Sineshchekov, O. A., Rodarte, E. M., Janz, R., Morelle, O., Melkonian, M., Wong, G. K.-S., & Spudich, J. L. (2017). The Expanding Family of Natural Anion Channelrhodopsins Reveals Large Variations in Kinetics, Conductance, and Spectral Sensitivity. *Scientific Reports*, *7*(1), 43358. https://doi.org/10.1038/srep43358

Govorunova, E. G., Sineshchekov, O. A., & Spudich, J. L. (2016). Proteomonas sulcata ACR1: A Fast Anion Channelrhodopsin. *Photochemistry and Photobiology*, *92*(2), 257–263. https://doi.org/10.1111/php.12558

Gradinaru, V., Mogri, M., Thompson, K., Henderson, J., & Deisseroth, K. (2009). Optical Deconstruction of Parkinsonian Neural Circuitry. *Science (New York, N.Y.)*, *324*, 354–9. https://doi.org/10.1126/science.1167093

Gradinaru, V., Thompson, K. R., & Deisseroth, K. (2008). eNpHR: A Natronomonas halorhodopsin enhanced for optogenetic applications. *Brain cell biology*, *36*(1-4), 129–139. https://doi.org/10.1007/s11068-008-9027-6

Grimm, C., Silapetere, A., Vogt, A., Bernal Sierra, Y. A., & Hegemann, P. (2018). Electrical properties, substrate specificity and optogenetic potential of the engineered light-driven sodium pump eKR2. *Scientific Reports*, *8*(1), 9316. https://doi.org/10.1038/s41598-018-27690-w

Grosenick, L., Marshel, J. H., & Deisseroth, K. (2015). Closed-loop and activity-guided optogenetic control. *Neuron*, *86*(1), 106–139. https://doi.org/10.1016/j.neuron.2015.03.034

Gross, C., Saponaro, A., Santoro, B., Moroni, A., Thiel, G., & Hamacher, K. (2018). Mechanical transduction of cytoplasmic-to-transmembrane-domain movements in a hyperpolarization-activated cyclic nucleotide-gated cation channel. *The Journal of Biological Chemistry*, *293*(33), 12908–12918. https://doi.org/10.1074/jbc.RA118.002139

Hamill, O. P., Marty, A., Neher, E., Sakmann, B., & Sigworth, F. J. (1981). Improved patch-clamp techniques for high-resolution current recording from cells and cell-free membrane patches. *Pflugers Archiv: European Journal of Physiology*, *391*(2), 85–100. https://doi.org/10.1007/BF00656997

Han, X., & Boyden, E. S. (2007). Multiple-Color Optical Activation, Silencing, and Desynchronization of Neural Activity, with Single-Spike Temporal Resolution. *PLOS ONE*, *2*(3), e299. https://doi.org/10.1371/journal.pone.0000299

Hartwig, C., Bähre, H., Wolter, S., Beckert, U., Kaever, V., & Seifert, R. (2014). cAMP, cGMP, cCMP and cUMP concentrations across the tree of life: High cCMP and cUMP levels in astrocytes. *Neuroscience Letters*, *579*, 183–187. https://doi.org/10.1016/j.neulet.2014.07.019

Henß, T., Nagpal, J., Gao, S., Scheib, U., Pieragnolo, A., Hirschhäuser, A., Schneider-Warme, F., Hegemann, P., Nagel, G., & Gottschalk, A. (2022). Optogenetic tools for manipulation of cyclic nucleotides functionally coupled to cyclic nucleotide-gated channels. *British Journal of Pharmacology*, *179*(11), 2519–2537. https://doi.org/10.1111/bph.15445

Inoue, K., Ono, H., Abe-Yoshizumi, R., Yoshizawa, S., Ito, H., Kogure, K., & Kandori, H. (2013). A light-driven sodium ion pump in marine bacteria. *Nature Communications*, *4*(1), 1678. https://doi.org/10.1038/ncomms2689

Iyer, S. M., Montgomery, K. L., Towne, C., Lee, S. Y., Ramakrishnan, C., Deisseroth, K., & Delp, S. L. (2014). Virally mediated optogenetic excitation and inhibition of pain in freely moving nontransgenic mice. *NATURE BIOTECHNOLOGY*, *32*(3), 274–278. https://doi.org/10.1038/nbt.2834
Web of Science ID: WOS:000332819800026

Janovjak, H., Szobota, S., Wyart, C., Trauner, D., & Isacoff, E. Y. (2010). A light-gated, potassium-selective glutamate receptor for the optical inhibition of neuronal firing. *Nature Neuroscience*, *13*(8), 1027–1032. https://doi.org/10.1038/nn.2589

Kato, H. E., Zhang, F., Yizhar, O., Ramakrishnan, C., Nishizawa, T., Hirata, K., Ito, J., Aita, Y., Tsukazaki, T., Hayashi, S., Hegemann, P., Maturana, A. D., Ishitani, R., Deisseroth, K., & Nureki, O. (2012). Crystal structure of the channelrhodopsin light-gated cation channel. *Nature*, *482*(7385), 369–374. https://doi.org/10.1038/nature10870

Kaupp, U. B., & Seifert, R. (2002). Cyclic nucleotide-gated ion channels. *Physiological Reviews*, *82*(3), 769–824. https://doi.org/10.1152/physrev.00008.2002

Kesters, D., Brams, M., Nys, M., Wijckmans, E., Spurny, R., Voets, T., Tytgat, J., Kusch, J., & Ulens, C. (2015). Structure of the SthK carboxy-terminal region reveals a gating mechanism for cyclic nucleotide-modulated ion channels. *PloS One*, *10*(1), e0116369. https://doi.org/10.1371/journal.pone.0116369

Kim, J. Y., Jo, B., Jo, Y., & Cha, H. (2012). Improved production of biohydrogen in light-powered Escherichia coli by co-expression of proteorhodopsin and heterologous hydrogenase. *Microbial Cell Factories*, *11*(1), 2. https://doi.org/10.1186/1475-2859-11-2

Klapoetke, N. C., Murata, Y., Kim, S. S., Pulver, S. R., Birdsey-Benson, A., Cho, Y. K., Morimoto, T. K., Chuong, A. S., Carpenter, E. J., Tian, Z., Wang, J., Xie, Y., Yan, Z., Zhang, Y., Chow, B. Y., Surek, B., Melkonian, M., Jayaraman, V., Constantine-Paton, M., … Boyden, E. S. (2014). Independent optical excitation of distinct neural populations. *Nature Methods*, *11*(3), 338–346. https://doi.org/10.1038/nmeth.2836

Kleis, P., Paschen, E., Häussler, U., Bernal Sierra, Y. A., & Haas, C. A. (2022). Long-term in vivo application of a potassium channel-based optogenetic silencer in the healthy and epileptic mouse hippocampus. *BMC Biology*, *20*(1), 18. https://doi.org/10.1186/s12915-021-01210-1

Kleppisch, T., & Feil, R. (2009). cGMP signalling in the mammalian brain: Role in synaptic plasticity and behaviour. *Handbook of Experimental Pharmacology*, (191), 549–579. https://doi.org/10.1007/978-3-540-68964-5_24

Kondapuram, M., Frieg, B., Yüksel, S., Schwabe, T., Sattler, C., Lelle, M., Schweinitz, A., Schmauder, R., Benndorf, K., Gohlke, H., & Kusch, J. (2020, September 21). *Functional and structural characterization of interactions between opposite subunits in HCN pacemaker channels*. https://doi.org/10.1101/2020.09.21.305797

Kralik, J., van Wyk, M., Stocker, N., & Kleinlogel, S. (2022). Bipolar cell targeted optogenetic gene therapy restores parallel retinal signaling and high-level vision in the degenerated retina. *Communications Biology*, *5*, 1116. https://doi.org/10.1038/s42003-022-04016-1

Krook-Magnuson, E., Armstrong, C., Oijala, M., & Soltesz, I. (2013). On-demand optogenetic control of spontaneous seizures in temporal lobe epilepsy. *Nature Communications*, *4*(1), 1376. https://doi.org/10.1038/ncomms2376

Kuo, M. M.-C., Saimi, Y., Kung, C., & Choe, S. (2007). Patch Clamp and Phenotypic Analyses of a Prokaryotic Cyclic Nucleotide-gated K+ Channel Using Escherichia coli as a Host*. *Journal of Biological Chemistry*, *282*(33), 24294–24301. https://doi.org/10.1074/jbc.M703618200

Leopold, A. V., Chernov, K. G., & Verkhusha, V. V. (2018). Optogenetically controlled protein kinases for regulation of cellular signaling. *Chemical Society reviews*, *47*(7), 2454–2484. https://doi.org/10.1039/c7cs00404d

Li, M., Zhou, X., Wang, S., Michailidis, I., Gong, Y., Su, D., Li, H., Li, X., & Yang, J. (2017). Structure of a eukaryotic cyclic-nucleotide-gated channel. *Nature*, *542*, 60–65. https://doi.org/10.1038/nature20819

Li, X., Gutierrez, D. V., Hanson, M. G., Han, J., Mark, M. D., Chiel, H., Hegemann, P., Landmesser, L. T., & Herlitze, S. (2005). Fast noninvasive activation and inhibition of neural and network activity by vertebrate rhodopsin and green algae channelrhodopsin. *Proceedings of the National Academy of Sciences*, *102*(49), 17816–17821. https://doi.org/10.1073/pnas.0509030102

Lin, J. Y., Knutsen, P. M., Muller, A., Kleinfeld, D., & Tsien, R. Y. (2013). ReaChR: A red-shifted variant of channelrhodopsin enables deep transcranial optogenetic excitation. *Nature Neuroscience*, *16*(10), 1499–1508. https://doi.org/10.1038/nn.3502

Lin, S., Du, Y., Xia, Y., Xie, Y., Xiao, L., & Wang, G. (2022). Advances in optogenetic studies of depressive-like behaviors and underlying neural circuit mechanisms. *Frontiers in Psychiatry*, *13*, 950910. https://doi.org/10.3389/fpsyt.2022.950910

Lolicato, M., Nardini, M., Gazzarrini, S., Möller, S., Bertinetti, D., Herberg, F. W., Bolognesi, M., Martin, H., Fasolini, M., Bertrand, J. A., Arrigoni, C., Thiel, G., & Moroni, A. (2011). Tetramerization dynamics of C-terminal domain underlies isoform-specific cAMP gating in hyperpolarization-activated cyclic nucleotide-gated channels. *The Journal of Biological Chemistry*, *286*(52), 44811–44820. https://doi.org/10.1074/jbc.M111.297606

Mahn, M., Gibor, L., Patil, P., Cohen-Kashi Malina, K., Oring, S., Printz, Y., Levy, R., Lampl, I., & Yizhar, O. (2018). High-efficiency optogenetic silencing with soma-targeted anion-conducting channelrhodopsins. *Nature Communications*, *9*(1), 4125. https://doi.org/10.1038/s41467-018-06511-8

Mahn, M., Saraf-Sinik, I., Patil, P., Pulin, M., Bitton, E., Karalis, N., Bruentgens, F., Palgi, S., Gat, A., Dine, J., Wietek, J., Davidi, I., Levy, R., Litvin, A., Zhou, F., Sauter, K., Soba, P., Schmitz, D., Lüthi, A., … Yizhar, O. (2021). Efficient optogenetic silenc-

ing of neurotransmitter release with a mosquito rhodopsin. *Neuron*, *109*(10), 1621–1635.e8. https://doi.org/10.1016/j.neuron.2021.03.013

Mansouri, M., Strittmatter, T., & Fussenegger, M. (2019). Light-Controlled Mammalian Cells and Their Therapeutic Applications in Synthetic Biology. *Advanced Science*, *6*(1), 1800952. https://doi.org/10.1002/advs.201800952

Marchesi, A., Gao, X., Adaixo, R., Rheinberger, J., Stahlberg, H., Nimigean, C., & Scheuring, S. (2018). An iris diaphragm mechanism to gate a cyclic nucleotide-gated ion channel. *Nature Communications*, *9*(1), 3978. https://doi.org/10.1038/s41467-018-06414-8

Molleman, A. (2003). *Patch clamping: An introductory guide to patch clamp electrophysiology*. J. Wiley

Morgan, J., Evans, E., & Zagotta, W. (2019). Functional characterization and optimization of a bacterial cyclic nucleotide–gated channel. *Journal of Biological Chemistry*, *294*, jbc.RA119.007699. https://doi.org/10.1074/jbc.RA119.007699

Nagel, G., Ollig, D., Fuhrmann, M., Kateriya, S., Musti, A. M., Bamberg, E., & Hegemann, P. (2002). Channelrhodopsin-1: A light-gated proton channel in green algae. *Science (New York, N.Y.)*, *296*(5577), 2395–2398. https://doi.org/10.1126/science.1072068

Nagel, G., Szellas, T., Huhn, W., Kateriya, S., Adeishvili, N., Berthold, P., Ollig, D., Hegemann, P., & Bamberg, E. (2003). Channelrhodopsin-2, a directly light-gated cation-selective membrane channel. *Proceedings of the National Academy of Sciences*, *100*(24), 13940–13945. https://doi.org/10.1073/pnas.1936192100

Neher, E., Sakmann, B., & Steinbach, J. H. (1978). The extracellular patch clamp: A method for resolving currents through individual open channels in biological membranes. *Pflugers Archiv: European Journal of Physiology*, *375*(2), 219–228. https://doi.org/10.1007/BF00584247

Ng, L., Zhuang, M., Van Petegem, F., Li, Y., & Accili, E. (2019). Binding and structural asymmetry governs ligand sensitivity in a cyclic nucleotide-gated ion channel. *Journal of General Physiology*, *151*(10), 1190–1212. https://doi.org/10.1085/JGP.201812162

Ohlendorf, R., & Möglich, A. (2022). Light-regulated gene expression in Bacteria: Fundamentals, advances, and perspectives. *Frontiers in Bioengineering and Biotechnology*, *10*, 1029403. https://doi.org/10.3389/fbioe.2022.1029403

Pan, Y., Pohjolainen, E., Schmidpeter, P. A. M., Vaiana, A. C., Nimigean, C. M., Grubmüller, H., & Scheuring, S. (2023). Discrimination between cyclic nucleotides in a cyclic nucleotide-gated ion channel. *Nature Structural & Molecular Biology*, 1–9. https://doi.org/10.1038/s41594-023-00955-3

Paoletti, P., Young, E. C., & Siegelbaum, S. A. (1999). C-Linker of Cyclic Nucleotide–gated Channels Controls Coupling of Ligand Binding to Channel Gating. *Journal of General Physiology*, *113*(1), 17–34. https://doi.org/10.1085/jgp.113.1.17

Raimondo, J. V., Kay, L., Ellender, T. J., & Akerman, C. J. (2012). Optogenetic silencing strategies differ in their effects on inhibitory synaptic transmission. *Nature Neuroscience*, *15*(8), 1102–1104. https://doi.org/10.1038/nn.3143

Rajasethupathy, P., Sankaran, S., Marshel, J. H., Kim, C. K., Ferenczi, E., Lee, S. Y., Berndt, A., Ramakrishnan, C., Jaffe, A., Lo, M., Liston, C., & Deisseroth, K. (2015). Projections from neocortex mediate top-down control of memory retrieval. *Nature*, *526*(7575), 653–659. https://doi.org/10.1038/nature15389

Reshetnikov, V. V., Smolskaya, S. V., Feoktistova, S. G., & Verkhusha, V. V. (2022). Optogenetic approaches in biotechnology and biomaterials. *Trends in Biotechnology*, *40*(7), 858–874. https://doi.org/10.1016/j.tibtech.2021.12.007

Rheinberger, J., Gao, X., Schmidpeter, P. A. M., & Nimigean, C. (2018). Ligand discrimination and gating in cyclic nucleotide-gated ion channels from apo and partial agonist-bound cryo-EM structures. *eLife*, *7*, null. https://doi.org/10.7554/eLife.39775

Rich, T. C., Tse, T. E., Rohan, J. G., Schaack, J., & Karpen, J. W. (2001). In Vivo Assessment of Local Phosphodiesterase Activity Using Tailored Cyclic Nucleotide–Gated Channels as Camp Sensors. *Journal of General Physiology*, *118*(1), 63–78. https://doi.org/10.1085/jgp.118.1.63

Sayegh, F. J. P., Mouledous, L., Macri, C., Pi Macedo, J., Lejards, C., Rampon, C., Verret, L., & Dahan, L. (2024). Ventral tegmental area dopamine projections to the hippocampus trigger long-term potentiation and contextual learning. *Nature Communications*, *15*(1), 4100. https://doi.org/10.1038/s41467-024-47481-4

Scheib, U., Broser, M., Constantin, O. M., Yang, S., Gao, S., Mukherjee, S., Stehfest, K., Nagel, G., Gee, C. E., & Hegemann, P. (2018). Rhodopsin-cyclases for photocontrol of cGMP/cAMP and 2.3 Å structure of the adenylyl cyclase domain. *Nature Communications*, *9*(1), 2046. https://doi.org/10.1038/s41467-018-04428-w

Schindelin, J., Arganda-Carreras, I., Frise, E., Kaynig, V., Longair, M., Pietzsch, T., Preibisch, S., Rueden, C., Saalfeld, S., Schmid, B., Tinevez, J.-Y., White, D. J., Hartenstein, V., Eliceiri, K., Tomancak, P., & Cardona, A. (2012). Fiji: An open-source platform for biological-image analysis. *Nature Methods*, *9*(7), 676–682. https://doi.org/10.1038/nmeth.2019

Schladt, T. (2022, March 28). *Gating of the Hv1 proton channel* [Thesis]. Universitäts- und Landesbibliothek Bonn

Schmidpeter, P. A. M., Gao, X., Uphadyay, V., Rheinberger, J., & Nimigean, C. (2018). Ligand binding and activation properties of the purified bacterial cyclic nucleotide–gated channel SthK. *The Journal of General Physiology*, *150*, 821–834. https://doi.org/10.1085/jgp.201812023

Schmidpeter, P. A. M., & Nimigean, C. . (2021). Correlating ion channel structure and function. *Methods in Enzymology*, *652*, 3–30. https://doi.org/10.1016/bs.mie.2021.02.016

Schmidpeter, P. A. M., Rheinberger, J., & Nimigean, C. (2020). Prolyl isomerization controls activation kinetics of a cyclic nucleotide-gated ion channel. *Nature Communications*, *11*, null. https://doi.org/10.1038/s41467-020-20104-4

Scholl, H. P. N., Strauss, R. W., Singh, M. S., Dalkara, D., Roska, B., Picaud, S., & Sahel, J.-A. (2016). Emerging therapies for inherited retinal degeneration. *Science Translational Medicine*, *8*(368), 368rv6–368rv6. https://doi.org/10.1126/scitranslmed.aaf2838

Shimizu-Sato, S., Huq, E., Tepperman, J. M., & Quail, P. H. (2002). A light-switchable gene promoter system. *Nature Biotechnology*, *20*(10), 1041–1044. https://doi.org/10.1038/nbt734

Sigworth, F. J., & Neher, E. (1980). Single Na+ channel currents observed in cultured rat muscle cells. *Nature*, *287*(5781), 447–449. https://doi.org/10.1038/287447a0

Sineshchekov, O. A., Govorunova, E. G., Li, H., & Spudich, J. L. (2015). Gating mechanisms of a natural anion channelrhodopsin. *Proceedings of the National Academy of Sciences*, *112*(46), 14236–14241. https://doi.org/10.1073/pnas.1513602112

Sørensen, A. T., Ledri, M., Melis, M., Nikitidou Ledri, L., Andersson, M., & Kokaia, M. (2018). Altered Chloride Homeostasis Decreases the Action Potential Threshold and Increases Hyperexcitability in Hippocampal Neurons. *eNeuro*, *4*(6), ENEURO.0172–17.2017. https://doi.org/10.1523/ENEURO.0172-17.2017

Stabel, R., Stüven, B., Hansen, J. N., Körschen, H. G., Wachten, D., & Möglich, A. (2019). Revisiting and Redesigning Light-Activated Cyclic-Mononucleotide Phosphodiesterases. *Journal of Molecular Biology*, *431*(17), 3029–3045. https://doi.org/10.1016/j.jmb.2019.07.011

Staley, K. J., Soldo, B. L., & Proctor, W. R. (1995). Ionic Mechanisms of Neuronal Excitation by Inhibitory GABAA Receptors. *Science*, *269*(5226), 977–981. https://doi.org/10.1126/science.7638623

Swanson, J. L., Chin, P.-S., Romero, J. M., Srivastava, S., Ortiz-Guzman, J., Hunt, P. J., & Arenkiel, B. R. (2022). Advancements in the Quest to Map, Monitor, and Manipulate Neural Circuitry. *Frontiers in Neural Circuits*, *16*. https://doi.org/10.3389/fncir.2022.886302

Szabadics, J., Varga, C., Molnár, G., Oláh, S., Barzó, P., & Tamás, G. (2006). Excitatory effect of GABAergic axo-axonic cells in cortical microcircuits. *Science (New York, N.Y.)*, *311*(5758), 233–235. https://doi.org/10.1126/science.1121325

Tan, P., He, L., Huang, Y., & Zhou, Y. (2022). Optophysiology: Illuminating cell physiology with optogenetics. *Physiological Reviews*, *102*(3), 1263–1325. https://doi.org/10.1152/physrev.00021.2021

Tian, Y., Yang, S., & Gao, S. (2020). Advances, Perspectives and Potential Engineering Strategies of Light-Gated Phosphodiesterases for Optogenetic Applications. *International Journal of Molecular Sciences*, *21*(20), 7544. https://doi.org/10.3390/ijms21207544

Tsunoda, S. P., Prigge, M., Abe-Yoshizumi, R., Inoue, K., Kozaki, Y., Ishizuka, T., Yawo, H., Yizhar, O., & Kandori, H. (2017). Functional characterization of sodium-pumping rhodopsins with different pumping properties. *PLOS ONE*, *12*(7), e0179232. https://doi.org/10.1371/journal.pone.0179232

Turecek, R., & Trussell, L. O. (2001). Presynaptic glycine receptors enhance transmitter release at a mammalian central synapse. *Nature*, *411*(6837), 587–590. https://doi.org/10.1038/35079084

Tye, K. M., & Deisseroth, K. (2012). Optogenetic investigation of neural circuits underlying brain disease in animal models. *Nature Reviews Neuroscience*, *13*(4), 251–266. https://doi.org/10.1038/nrn3171

Tye, K. M., Prakash, R., Kim, S.-Y., Fenno, L. E., Grosenick, L., Zarabi, H., Thompson, K. R., Gradinaru, V., Ramakrishnan, C., & Deisseroth, K. (2011). Amygdala circuitry

mediating reversible and bidirectional control of anxiety. *Nature*, *471*(7338), 358–362. https://doi.org/10.1038/nature09820

Valverde, S., Vandecasteele, M., Piette, C., Derousseaux, W., Gangarossa, G., Aristieta Arbelaiz, A., Touboul, J., Degos, B., & Venance, L. (2020). Deep brain stimulation-guided optogenetic rescue of parkinsonian symptoms. *Nature Communications*, *11*(1), 2388. https://doi.org/10.1038/s41467-020-16046-6

Varnum, M. D., Black, K. D., & Zagotta, W. N. (1995). Molecular mechanism for ligand discrimination of cyclic nucleotide-gated channels. *Neuron*, *15*(3), 619–625. https://doi.org/10.1016/0896-6273(95)90150-7

Vialou, V., Bagot, R. C., Cahill, M. E., Ferguson, D., Robison, A. J., Dietz, D. M., Fallon, B., Mazei-Robison, M., Ku, S. M., Harrigan, E., Winstanley, C. A., Joshi, T., Feng, J., Berton, O., & Nestler, E. J. (2014). Prefrontal Cortical Circuit for Depression- and Anxiety-Related Behaviors Mediated by Cholecystokinin: Role of ΔFosB. *Journal of Neuroscience*, *34*(11), 3878–3887. https://doi.org/10.1523/JNEUROSCI.1787-13.2014

Vierock, J., Peter, E., Grimm, C., Rozenberg, A., Chen, I.-W., Tillert, L., Castro Scalise, A. G., Casini, M., Augustin, S., Tanese, D., Forget, B. C., Peyronnet, R., Schneider-Warme, F., Emiliani, V., Béjà, O., & Hegemann, P. (2022). WiChR, a highly potassium-selective channelrhodopsin for low-light one- and two-photon inhibition of excitable cells. *Science Advances*, *8*(49), eadd7729. https://doi.org/10.1126/sciadv.add7729

Wettschureck, N., & Offermanns, S. (2005). Mammalian G Proteins and Their Cell Type Specific Functions. *Physiological Reviews*, *85*(4), 1159–1204. https://doi.org/10.1152/physrev.00003.2005

Wietek, J., Beltramo, R., Scanziani, M., Hegemann, P., Oertner, T. G., & Wiegert, J. S. (2015). An improved chloride-conducting channelrhodopsin for light-induced inhibition of neuronal activity in vivo. *Scientific Reports*, *5*(1), 14807. https://doi.org/10.1038/srep14807

Wietek, J., Wiegert, J. S., Adeishvili, N., Schneider, F., Watanabe, H., Tsunoda, S. P., Vogt, A., Elstner, M., Oertner, T. G., & Hegemann, P. (2014). Conversion of Channelrhodopsin into a Light-Gated Chloride Channel. *Science*, *344*(6182), 409–412. https://doi.org/10.1126/science.1249375

Wobig, L. (2021, April 29). *Characterization of the hyperpolarization-activated, highly-selective proton channel HCNL1 found in the sperm of the zebrafish Danio rerio* [Thesis]. Universitäts- und Landesbibliothek Bonn.
Accepted: 2021-04-29T09:00:48Z

Woo, J., Im, S.-K., Chun, H., Jung, S.-Y., Oh, S.-J., Choi, N., Lee, C. J., & Hur, E.-M. (2017). Functional Characterization of Resting and Adenovirus-Induced Reactive Astrocytes in Three-Dimensional Culture. *Experimental Neurobiology*, *26*(3), 158–167. https://doi.org/10.5607/en.2017.26.3.158

Xie, Y.-f., Jackson, M. F., & MacDonald, J. F. (2013). Optogenetics and synaptic plasticity. *Acta Pharmacologica Sinica*, *34*(11), 1381–1385. https://doi.org/10.1038/aps.2013.150

Xu, X., Vysotskaya, Z. V., Liu, Q., & Zhou, L. (2010). Structural Basis for the cAMP-dependent Gating in the Human HCN4 Channel*. *Journal of Biological Chemistry*, *285*(47), 37082–37091. https://doi.org/10.1074/jbc.M110.152033

Ye, H., Baba, M. D.-E., Peng, R.-W., & Fussenegger, M. (2011). A Synthetic Optogenetic Transcription Device Enhances Blood-Glucose Homeostasis in Mice. *Science*, *332*(6037), 1565–1568. https://doi.org/10.1126/science.1203535

Yi, J. J., Wang, H., Vilela, M., Danuser, G., & Hahn, K. M. (2014). Manipulation of Endogenous Kinase Activity in Living Cells Using Photoswitchable Inhibitory Peptides. *ACS Synthetic Biology*, *3*(11), 788–795. https://doi.org/10.1021/sb5001356

Yizhar, O., Fenno, L. E., Davidson, T. J., Mogri, M., & Deisseroth, K. (2011). Optogenetics in neural systems. *Neuron*, *71*(1), 9–34. https://doi.org/10.1016/j.neuron.2011.06.004

Zachariou, V., & Carr, F. P. (2014). Nociception and pain: Lessons from optogenetics. *Frontiers in Behavioral Neuroscience*, *8*. https://doi.org/10.3389/fnbeh.2014.00069

Zagotta, W. N., Olivier, N. B., Black, K. D., Young, E. C., Olson, R., & Gouaux, E. (2003). Structural basis for modulation and agonist specificity of HCN pacemaker channels. *Nature*, *425*(6954), 200–205. https://doi.org/10.1038/nature01922

Zhang, F., Wang, L.-P., Brauner, M., Liewald, J. F., Kay, K., Watzke, N., Wood, P. G., Bamberg, E., Nagel, G., Gottschalk, A., & Deisseroth, K. (2007). Multimodal fast optical interrogation of neural circuitry. *Nature*, *446*(7136), 633–639. https://doi.org/10.1038/nature05744

Zheng, X., Fu, Z., Su, D., Zhang, Y., Li, M.-h., Pan, Y., Li, H., Li, S., Grassucci, R., Ren, Z., Hu, Z., Li, X., Zhou, M., Li, G., Frank, J., & Yang, J. (2020). Mechanism of ligand activation of a eukaryotic cyclic nucleotide-gated channel. *Nature structural & molecular biology*, *27*, 625–634. https://doi.org/10.1038/s41594-020-0433-5

Zhou, X., Wang, J., Chen, J., Qi, Y., Di Nan, n., Jin, L., Qian, X., Wang, X., Chen, Q., Liu, X., & Xu, Y. (2018). Optogenetic control of epithelial-mesenchymal transition in cancer cells. *Scientific Reports*, *8*(1), 14098. https://doi.org/10.1038/s41598-018-32539-3

Zhou, Z., Wang, X., Li, X., & Liao, L. (2023). A bibliometric profile of optogenetics: Quantitative and qualitative analyses. *Frontiers in Neuroscience*, *17*. https://doi.org/10.3389/fnins.2023.1221316

Zong, X., Zucker, H., Hofmann, F., & Biel, M. (1998). Three amino acids in the C-linker are major determinants of gating in cyclic nucleotide-gated channels. *The EMBO journal*, *17*(2), 353–362. https://doi.org/10.1093/emboj/17.2.353

9 Acknowledgement

I am filled with immense gratitude for Dr. Reinhard Seifert, whose pivotal role in my thesis journey has been truly transformative. His unwavering support, thoughtful care, enlightening scientific discussions, and patient guidance have significantly shaped the trajectory of my research. I genuinely appreciate the invaluable opportunity he has provided me to undertake this thesis

I am also deeply grateful to Dr. Heinz Beck for his pivotal role as my TAC member, his comprehensive review of my work, our collaborative efforts on RoCK 2.1 in vivo experiments, and his invaluable suggestions. I would also like to express my gratitude to the lab members, especially Dr. Thoralf Opitz and Lea Adenauer, for their unwavering support and guidance.

I want to express my gratitude to Prof. Dagmar Wachten for serving as my TAC member, inviting me to departmental meetings and journal clubs, and providing invaluable insights into my research. I also appreciate the support of the lab members; their expertise and willingness to share knowledge have greatly enriched my understanding and significantly contributed to the progress of my work.

I extend my sincere gratitude to Prof. Günter Mayer and Prof. Ute C. Vothknecht for their participation in my TAC committee. Their scientific insights and unwavering support have been invaluable to my research.

I deeply appreciate the unique expertise and support provided by Dr. Wolfgang Bönigk and Dr. Heinz Körschen, whose contributions and advice have significantly contributed to the success of this project.

Special thanks are also due to Jessica Goergen, and Norbert Brenner for their exceptional technical support and the positive atmosphere they fostered in the lab. Their assistance in cell culture and camaraderie have been indispensable.

I am grateful to Dr. Yinth Bernal Sierra, Anika Spreen, and Prof. Peter Hegemann for their collaboration on this project and for providing us with RoCK 2.1.

I acknowledge the Core Facility for Genetic Technology service at MPINB Bonn, Germany, and extend my thanks to the director and all staff members for their support and cooperation.

I am deeply grateful to my parents and friends, especially Krishna, Aman whose steadfast support has been an unwavering source of encouragement throughout my PhD journey.

This project was funded by the DFG Priority Program SPP 1926- Next Generation Optogenetics